Electronic Supplementary Material (ESI) for ChemComm.

Supporting Information

Spatially Resolved Fluoroalkylation and Alkylation of Graphene by Direct Laser Writing

Sabrin Al-Fogra, Sofia Rohde, Marcus Speck, Fank Hauke, Andreas Hirsch and Tao Wei,*

Department of Chemistry and Pharmacy & Center of Advance Materials and Processes (ZMP), Friedrich-Alexander University of Erlangen-Nürnberg, Nikolaus-Fiebiger-Strasse 10, 91058, Erlangen, Germany

E-mail: tao.wei@fau.de

Materials

CVD graphene on a 1×1 cm^2 polymethyl methacrylate (PMMA) substrate was purchased from ACS Material Co. (USA). All other chemicals were purchased from Sigma Aldrich Co. (Germany) and used without further treatment. Si/SiO_2 wafers (300 nm oxide layer) were purchased from Fraunhofer-Institute in Erlangen. Before use, the Si/SiO_2 wafers were cleaned by immersing them in isopropanol for ultrasonic treatment (300 W) for 5 min.

Raman Spectroscopy

The Raman spectroscopic characterization was performed on a Horiba Jobin Yvon LabRAM Aramis. A laser (Olympus LMPlanFl50x, NA 0.50) with an excitation wavelength of 532 nm, intensity of 8 mW, and a spot size of ~ 1 µm was used. The spectrometer was calibrated by using crystalline graphite. Spectral data was obtained through a motorized x-y table in a continuous line scan mode (SWIFT-module). The temperature-dependent Raman measurements were performed in a LinKAM stage THMS 600, equipped with a liquid nitrogen pump MS94 for temperature stabilization under a constant flow of nitrogen. The measurements were carried out on Si/SiO_2 wafers with a heating rate of 10 °C/min.

The Statistical Raman mappings were carried out on a confocal Raman microscope (WITec, alpha 300RA) using the green laser with an excitation wavelength of 532 nm, integration time of 1s, and the intensity of 2 mW.

Experimental Section

All chemicals used were of analytical grade and purchased from Aldrich Co. The solvents were purified before use by distillation. Analytical thin-layer chromatography (TLC) was performed on Merck silica gel (neutral, fluorescence indicator F254) precoated plates. ^{1}H NMR spectra were recorded at frequencies of 600 MHz (Bruker Ascend 600, probe head CPDCH600S3 C/H-D-05Z), carbon-13 spectra at 151 MHz. The NMR spectra of the fluorinated compounds were recorded at Bruker Ascend 500, probe head PATBO500S1BB-H/F-D-05ZFB, with frequencies of 471 MHz (^{19}F) and 126 MHz (^{13}C). All chemical shifts of ^{1}H and ^{13}C are given in ppm and have been converted to the δ scale and are referenced against the DMSO signal as an internal standard. The ^{19}F shifts are referenced against an externally measured C_6F_6 probe, δ=-164.9 ppm.

Synthesis of silver(I) perfluorocarboxylates

According to known procedures [1-3], silver(I) carbonate (7.4 mMol - 21.3 mMol) reacted with the equimolar amount of perfluorinated carboxylic acids (7.4 mMol - 21.3 mMol) under room temperature and in the absence of light in an aqueous ethanolic solution within 24 hours. After filtration, the precipitate was washed with ethanol and dried. (G_{F1} – G_{F8}).

Silver(I) perfluoropropanoate, C_3F_5-COOAg [509-09-1] (G_{F1})

Yield 4.78 g (80 %), δ_C (126 MHz, DMSO-d_6) 107.26, 119.13, 158.81 ppm; δ_F (471 MHz, DMSO-d_6) -84.06 (3F), -120.40 (2F) ppm.

Silver(I) perfluorobutanoate, C_3F_7-COOAg [3794-64-7] (G_{F2})

Yield 5.61 g (98 %), δ_C(126 MHz, DMSO-d_6) 108.78, 108.91, 117.81, 158.43 ppm; δ_F(471 MHz, DMSO-d_6) -82.46 (3F), -117.87 (2F), -128.52 (2F) ppm.

Silver(I) perfluoropentanoate, C_4F_9-COOAg [2795-30-4] (G_{F3})

Yield 4.65 g (94 %), δ_C (126 MHz, DMSO-d_6) 108.47, 109.22, 110.57, 117.21, 158.52 ppm; δ_F (471 MHz, DMSO-d_6) -82.92 (3F), -117.27 (2F), -125.01 (2F), -127.79 (2F) ppm.

Silver(I) perfluorohexanoate, C_5F_{11}-COOAg [336-02-7] (G_{F4})

Yield 4.62 g (98 %), δ_C (126 MHz, DMSO-d_6) 108.13, 109.28, 110.21, 111.04, 116.90, 158.33 ppm; δ_F (471 MHz, DMSO-d_6) -82.70 (3F), -117.09 (2F), -124.39 (2F), -124.60 (2F), -127.29 (2F) ppm.

Silver(I) perfluoroheptanoate, C_6F_{13}-COOAg [424-05-5] (G_{F5})
Yield 4.26 g (94 %), δ_C (126 MHz, DMSO-d_6) 108.00, 109.31, 109.03, 110.68, 111.13, 116.73, 158.35 ppm; δ_F (471 MHz, DMSO-d_6) -82.68 (3F), -117.07 (2F), -123.86 (2F), -124.20 (2F), -125.03 (2F), -128.17 (2F) ppm.

Silver(I) perfluorooctanoate, C_7F_{15}-COOAg [335-93-3] (G_{F6})
Yield 4.07 g (92 %), %), δ_C (126 MHz, DMSO-d_6) 107.89, 109.32, 109.81, 110.38, 110.74, 111.14, 116.62, 158.34 ppm; δ_F (471 MHz, DMSO-d_6) -82.67 (3F), -117.08 (2F), -123.70 (2F), -124.23 (b, 2 x 2F), -124.93 (2F), -128.18 (2F) ppm.

Silver(I) perfluorononanoate, C_8F_{17}-COOAg [7358-16-9] (G_{F7})
Yield 3.38 g (78 %), δ_C (126 MHz, DMSO-d_6) 107.86, 109.32, 109.72, 110.29, 110.46, 110.78, 111.17, 116.58, 158.32 ppm; δ_F (471 MHz, DMSO-d_6) -82.67 (3F), -117.09 (2F), -123.68 (2F), -124.16 (b, 3x2F), -124.91 (2F), -128.17 (2F) ppm.

Silver(I) perfluorodecanoate, C_9F_{19}-COOAg [5784-82-7] (G_{F8})
Yield 2.58 g (47 %), δ_C(126 MHz, DMSO-d_6) 107.82, 109.34, 109.67, 110.18, 110.33, 110.47, 110.78, 111.14, 116.54, 158.43 ppm; δ_F(471 MHz, DMSO-d_6) -82.96 (3F), -117.20 (2F), -123.81 (2F), -124.27 (b, 4x2F), -125.06 (2F), -128.38 (2F) ppm.

Synthesis of silver(I) carboxylates
According to known procedure [4,5], carboxylic acid (26.0 mMol – 48.3 mMol) was dissolved in the absence of light in the equimolar amount of 1M aqueous KOH (26.0 – 48.3 mMol), followed by the addition of an equimolar amount of 1M aqueous $AgNO_3$ solution. After 24 h stirring and subsequent filtration under vacuum, the precipitate was washed with ice cold water (55 mL – 90 mL) and dried. (G_{H1} – G_{H6}).

Silver(I) propanoate, C_2H_5-COOAg [5489-14-5] (G_{H1})
Yield 5.67 g (65 %), δ_H (600 MHz, DMSO-d_6) 0.99 (t, J 7.6 Hz, 3H, CH_3), 2.09 (q, J 7.6, 2H, CH_2) ppm; δ_C (151 MHz, DMSO-d_6) 11.29, 29.63, 177.72 ppm.

Silver(I) butanoate, C_3H_7-COOAg [5076-24-4] (G_{H2})
Yield 7.00 g (79 %), δ_H (600 MHz, DMSO-d_6) 0.86 (t, *J* 7.4 Hz, 3H, CH_3), 1.51 (tq (*pseudo*-hext), J 7.4 Hz, 2H, CH_2-CH_3), 2.08 (t, *J* 7.3, 2H, OOC-CH_2) ppm; δ_C (151 MHz, DMSO-d_6) 14.19, 19.71, 38.75, 176.96 ppm.

Silver(I) pentanoate, C_4H_9-COOAg [35363-46-3] (G_{H3})
Yield 6.50 g (81 %), δ_H (600 MHz, DMSO-d_6) 0.85 (t, *J* 7.4 Hz, 3H, CH_3), 1.27 (m, 2H, CH_2), 1.47 (m, 2H, CH_2), 2.09 (t, *J* 7.4, 2H, OOC-CH_2) ppm; δ_C (151 MHz, DMSO-d_6) 13.88, 22.21, 28.67, 36.36, 177.10 ppm.

Silver(I) hexanoate, C_5H_{11}-COOAg [32461-90-8] (G_{H4})
Yield 5.50 g (77 %), δ_H (600 MHz, DMSO-d_6) 0.85 (t, *J* 7.1 Hz, 3H, CH_3), 1.25 (m, 4H, 2xCH_2), 1.49 (m, 2H, CH_2), 2.07 (t, *J* 7.4, 2H, OOC-CH_2) ppm; δ_C (151 MHz, DMSO-d_6) 13.95, 22.04, 26.18, 31.42, 36.61, 177.10 ppm.

Silver(I) heptanoate, C_6H_{13}-COOAg [32461-91-9] (G_{H5})
Yield 5.46 g (73 %), δ_H (600 MHz, DMSO-d_6) 0.84 (t, *J* 7.0 Hz, 3H, CH_3), 1.24 (m, 6H, ,3xCH_2), 1.47 (m, 2H, CH_2), 2.07 (t, *J* 7.4, 2H, OOC-CH_2) ppm; δ_C (151 MHz, DMSO-d_6) 13.96, 22.08, 26.24, 28.78, 31.21, 36.29, 177.78 ppm.

Silver(I) octanoate, C_5H_{11}-COOAg [24927-67-1] (G_{H6})
Yield 6.49 g (91 %), δ_H (600 MHz, DMSO-d_6) 0.86 (t, *J* 7.0 Hz, 3H, CH_3), 1.26 (m, 8H, 4xCH_2), 1.49 (m, 2H, CH_2), 2.05 (t, *J* 7.4, 2H, OOC-CH_2) ppm; δ_C (151 MHz, DMSO-d_6) 13.67, 21.83, 26.24, 28.39, 28.94, 31.06, 36.28, 176.83 ppm.

2D-patterning of graphene via laser-writing. The Si/SiO_2 wafer was first cleaned by immersing it in isopropanol, followed by ultrasonic treatment (300 W) for 5 min. Then, a graphene monolayer was deposited to this wafer by a wet transfer technique. Here, the PMMA-supported graphene, floating on top of a water surface, was fished onto the prepared Si/SiO_2 wafer. The PMMA layer was easily removed by dissolution with acetone overnight. Afterward, the wafers were immersed in a solution of respective reagents (9 mmol/mL, see below for details) dissolved in isopropanol for 30 min. Subsequently, a drop of the solution was applied onto the wafer, respectively, resulting

in the generation of a thin and homogeneous crystalline film atop the graphene by evaporating the solvent with argon. The laser writing procedure was carried out using a green laser (λexc = 532 nm, 50x objective magnification, irradiation time 1s, 8mW) for the photolysis of the reactants. This process generates highly reactive fluoroalkylated and alkylated radicals that selectively bound to the underlying graphene exclusively in the laser-irradiated areas (Figure S1 and S2). Finally, washing away the excess reagents with isopropanol gives rise to the target-pattered graphene architectures. The employed photoactive compounds are: (I) fluoroalkyl silver carboxylates, including $C_3AgF_5O_2$, $C_4AgF_7O_2$, $C_5AgF_9O_2$, $C_6AgF_{11}O_2$, $C_7AgF_{13}O_2$, $C_8AgF_{15}O_2$, $C_8AgF_{15}O_2$, and $C_8AgF_{15}O_2$, and (II) alkyl silver carboxylates containing $C_3H_5AgO_2$, $C_4H_7AgO_2$, $C_5H_9AgO_2$, $C_6H_{11}AgO_2$, $C_7H_{13}AgO_2$, and $C_8H_{15}AgO_2$.

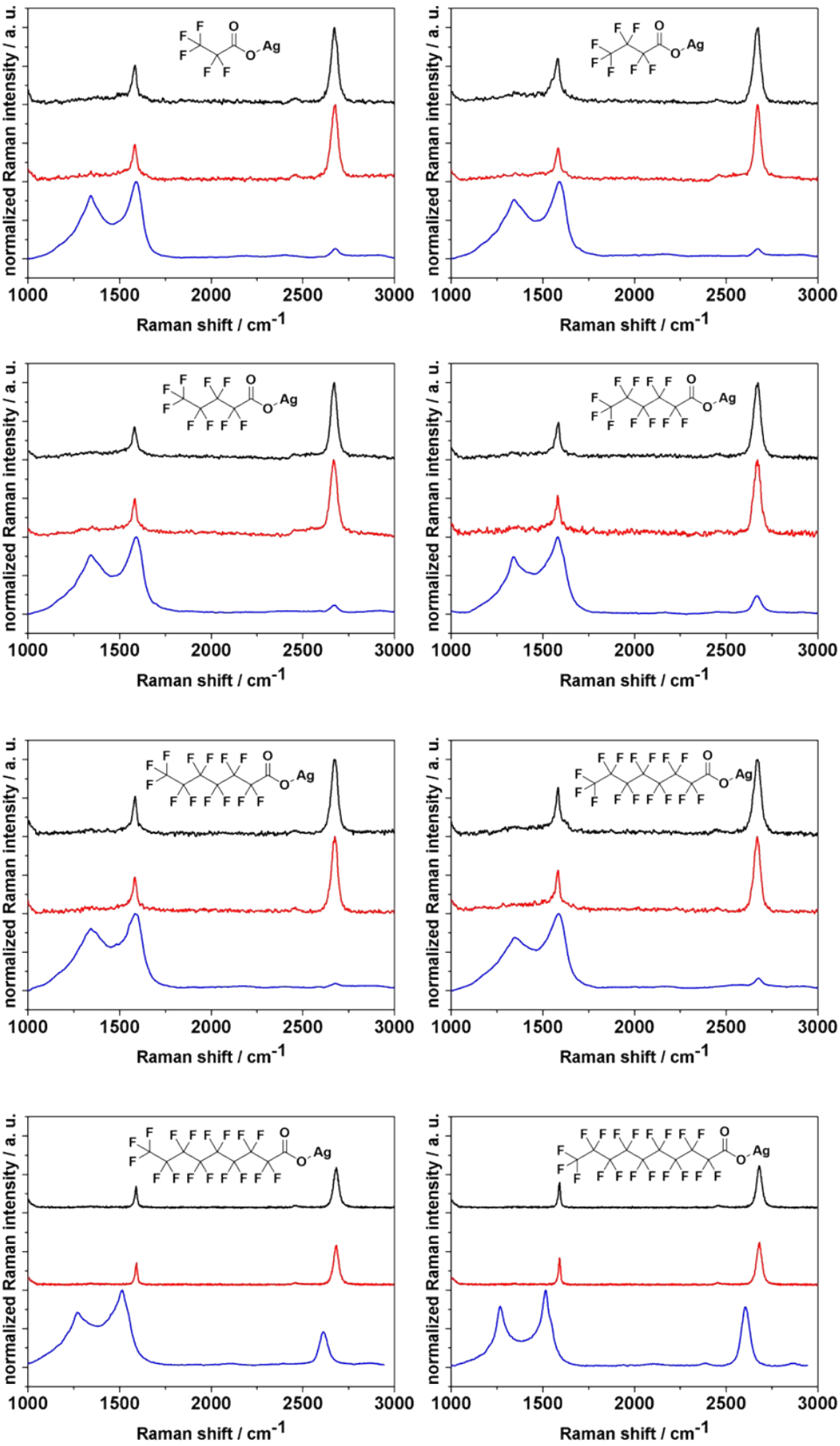

Figure S1. Normalized mean Raman spectra of pristine graphene (black line), non-irradiated areas (red line), and irradiated areas of samples $\mathbf{G_{F1}}$-$\mathbf{G_{F8}}$ (blue line).

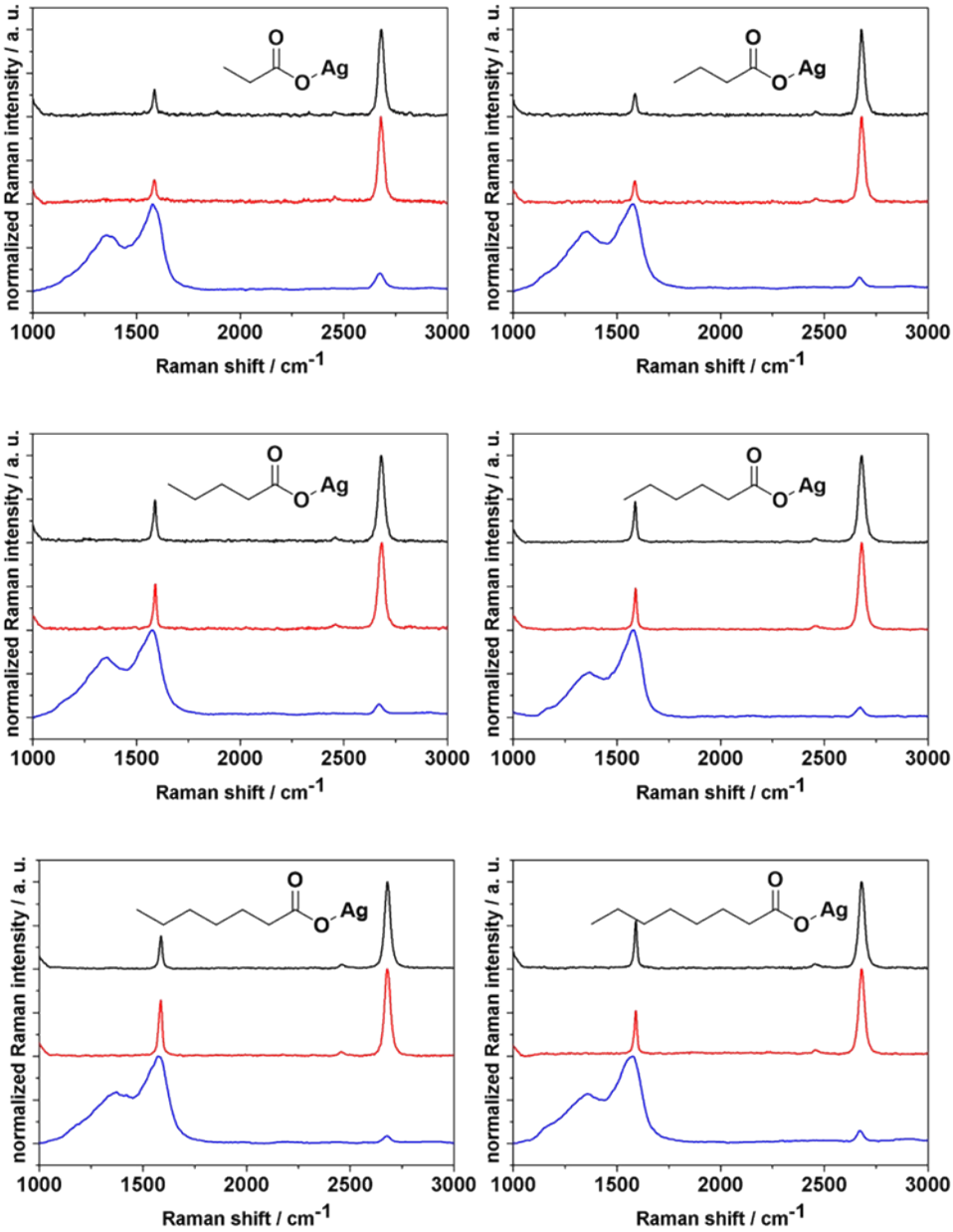

Figure S2. Normalized mean Raman spectra of pristine graphene (black line), non-irradiated areas (red line), and irradiated areas of samples $\mathbf{G_{H1}}$-$\mathbf{G_{H6}}$ (blue line).

Temperature-Dependent Raman analysis. Temperature-dependent Raman spectroscopy measurements were conducted to investigate the thermal stability of the addend binding in the fluoroalkylated graphene (Figure S3) and alkylated graphene (Figure S4). The temperature-dependent Raman measurements were performed in a Linkam state, equipped with a liquid nitrogen pump for temperature stabilization under a constant flow of nitrogen to determine the thermal stability and the reversibility of the covalent addend binding. The measurements were carried out on Si/SiO_2 wafers with a heating rate of 10 °C/min and the developments of the Raman-specific bands were recorded. For samples $\mathbf{G_{F1}}$-$\mathbf{G_{F8}}$, as the temperature rises to 350°C, the I_D/I_G ratio shows a continuous increase, reaching a value of approximate 1.0 (Figure S3). Overall, the behavior of all samples is very similar, with a maximum I_D/I_G ratio of 0.95 - 1.0. However, a further increase in the temperature to 400°C leads to a sharp decline of the D band, resulting in an I_D/I_G ratio < 0.1, indicative of complete defunctionalization. As such, the intact sp^2-carbon lattice of graphene is restored. Samples $\mathbf{G_{H1}}$-$\mathbf{G_{H6}}$ exhibit a similar trend in D-peak behavior during heat treatments below 350 °C, where the intensity of the D-peak continuously increases with rising temperature until the I_D/I_G ratio reaches 0.9 (Figure S4). A further increase of the temperature to 400 °C results in the complete disappearance of the D-, G-, and 2D-band. This suggests that, unlike $\mathbf{G_{H1}}$-$\mathbf{G_{H6}}$, the high-temperature processing leads to the disintegration of the graphene network rather than the cleavage of the bond between graphene and addends.

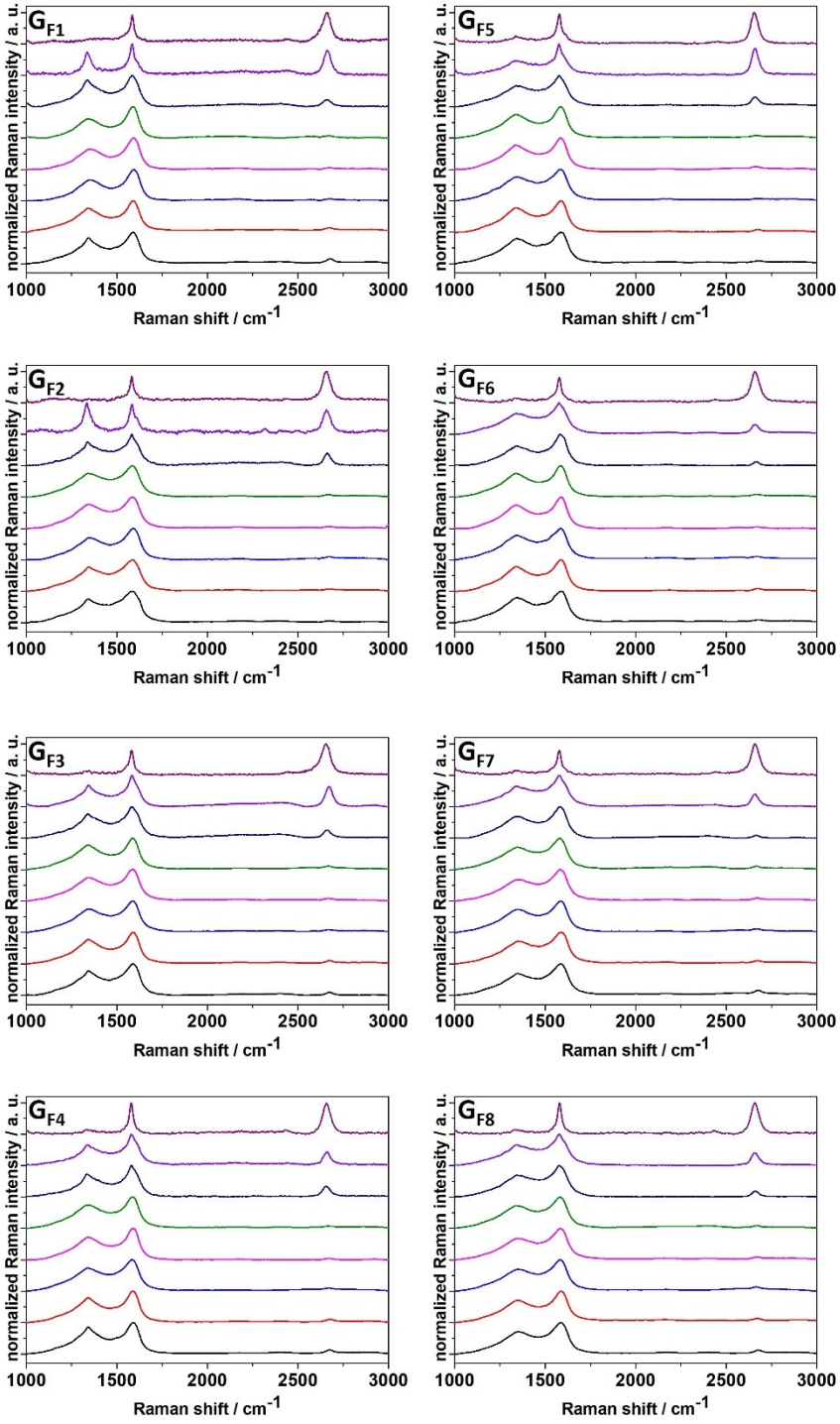

Figure S3. Temperature-dependent Raman spectra of samples G_{F1}-G_{F8}.

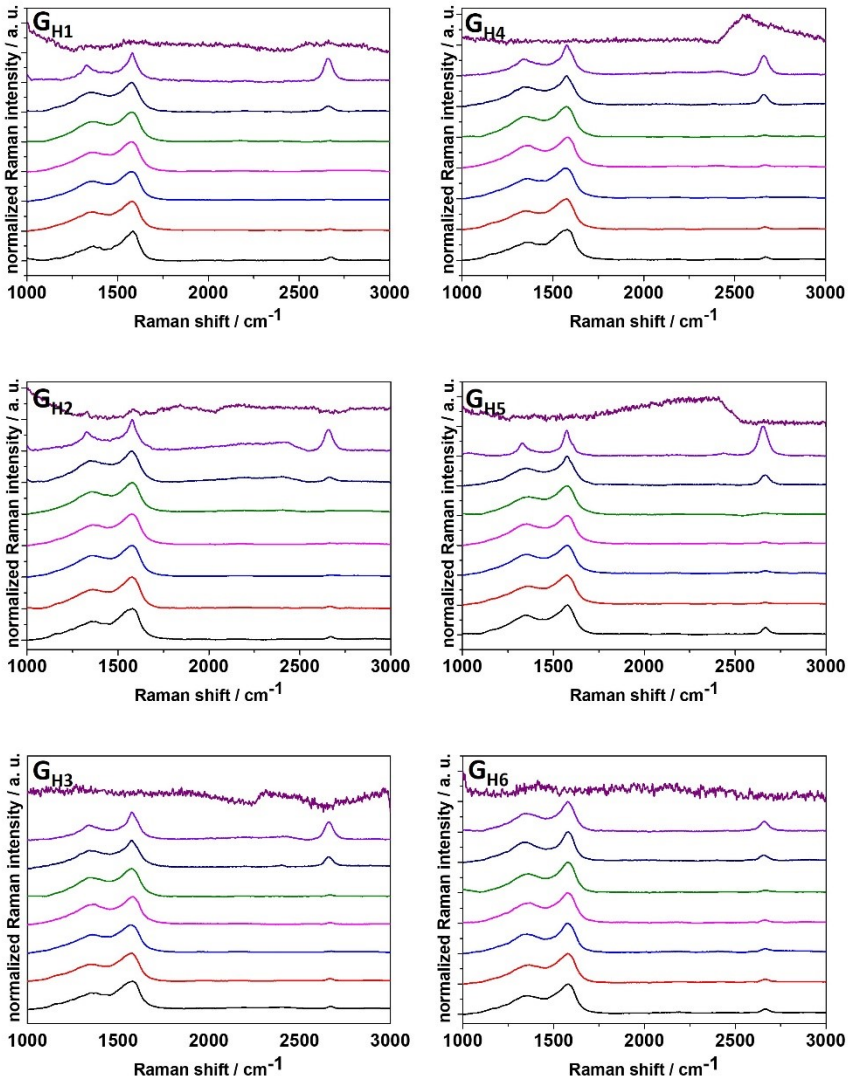

Figure S4. Temperature-dependent Raman spectra of samples G_{H1}-G_{H6}.

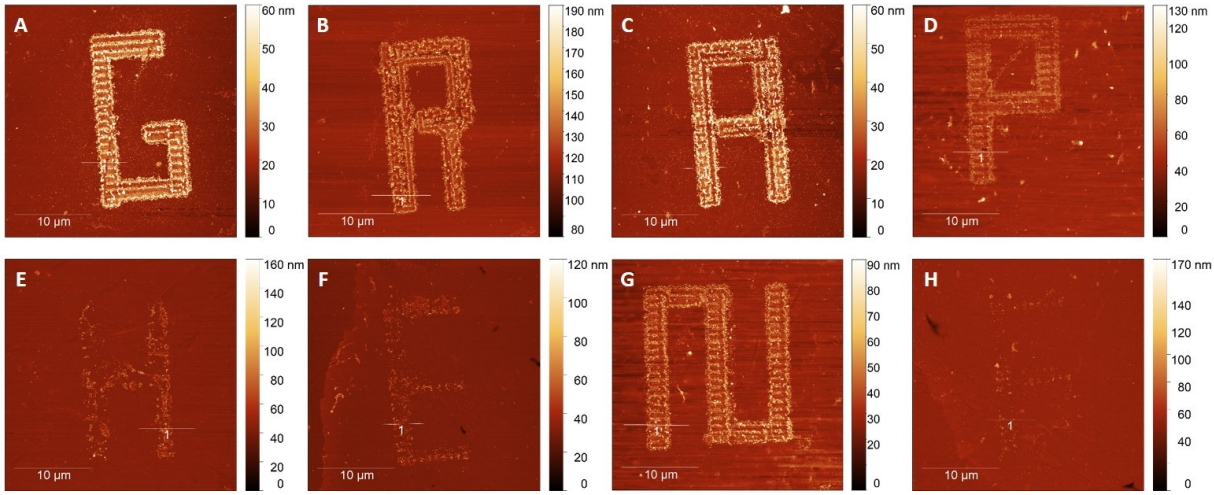

Figure S5. AFM images of the samples $\mathbf{G_{F1}}$ (A), $\mathbf{G_{F2}}$ (B), $\mathbf{G_{F3}}$ (C), $\mathbf{G_{F4}}$ (D), $\mathbf{G_{F5}}$ (E), $\mathbf{G_{F6}}$ (F), $\mathbf{G_{F7}}$ (G), and $\mathbf{G_{F8}}$ (H).

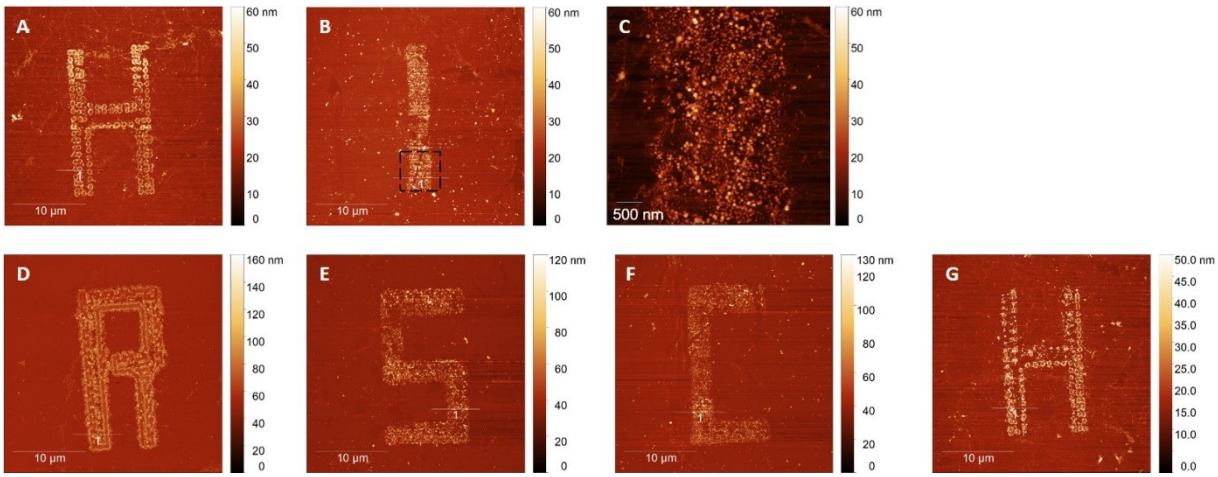

Figure S6. AFM images of the samples $\mathbf{G_{H1}}$ (A), $\mathbf{G_{H2}}$ (B), $\mathbf{G_{H3}}$ (D), $\mathbf{G_{H4}}$ (E), $\mathbf{G_{H5}}$ (F), and $\mathbf{G_{H6}}$ (G), and AFM image of the zoomed-in region marked by a black square (C).

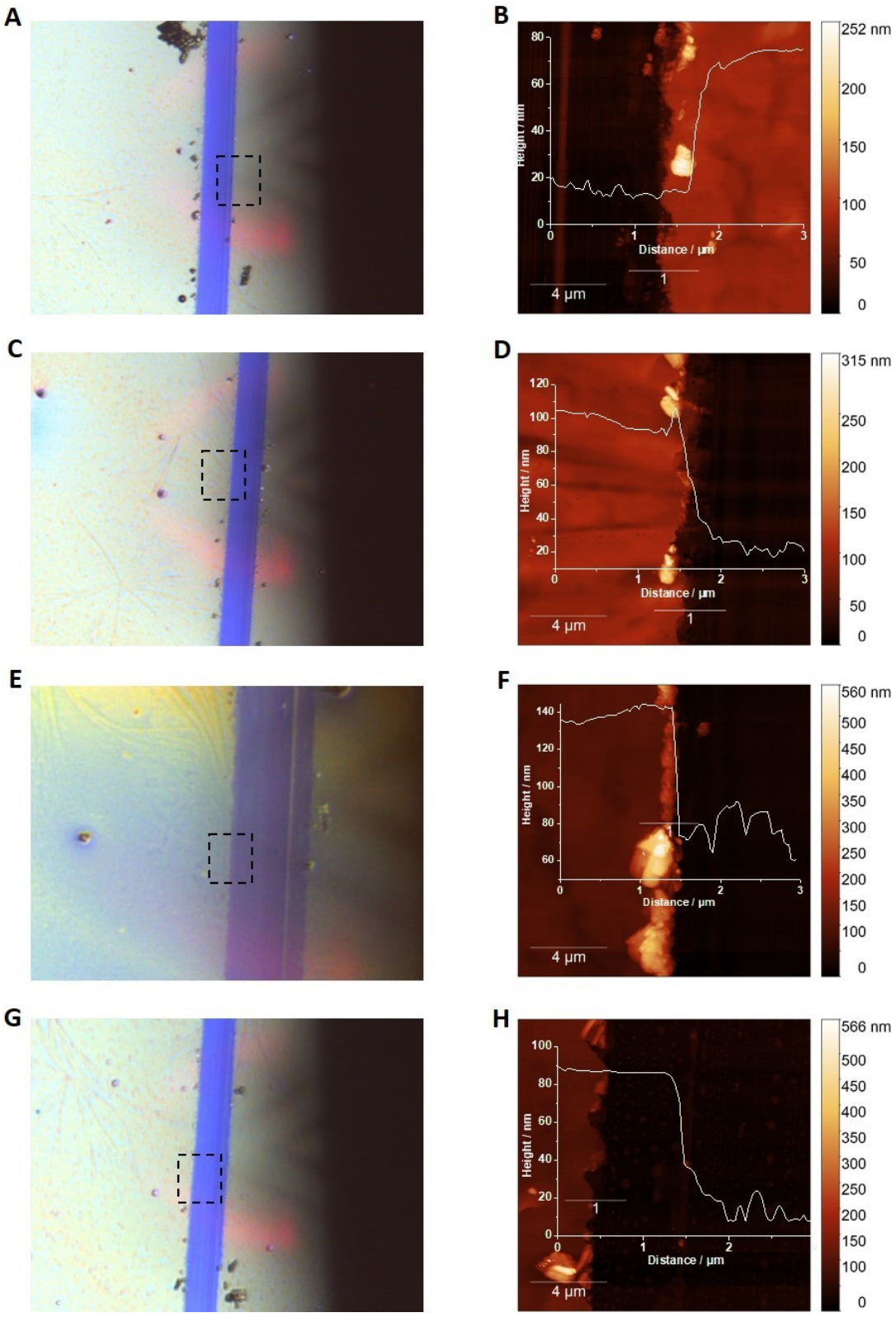
A
B
C
D
E
F
G
H
Height / nm
Distance / µm
4 µm
252 nm
315 nm
560 nm
566 nm

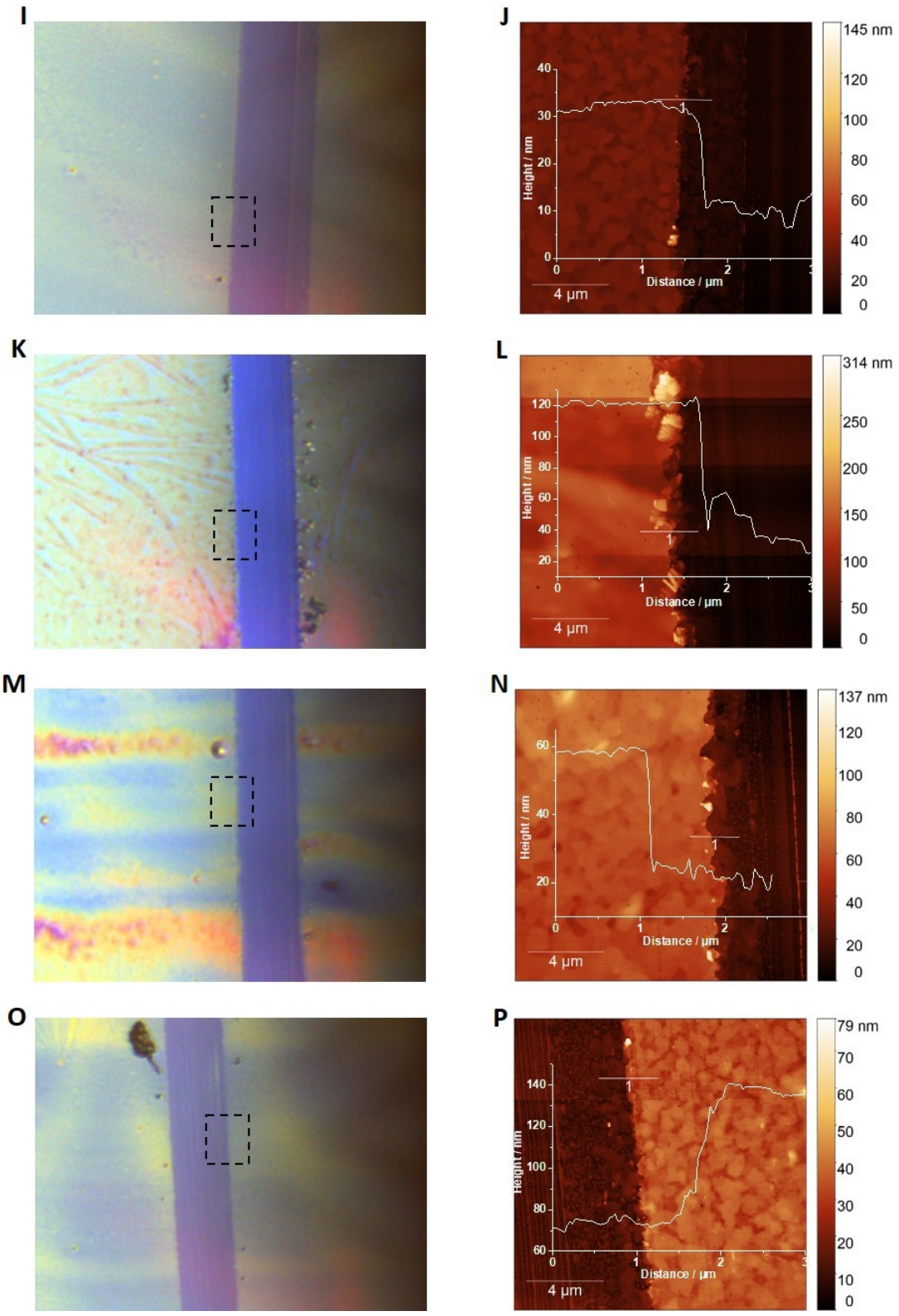

Figure S7. Optical images and corresponding AFM images of precursor film in samples $\mathbf{G_{F1}}$ (A, B), $\mathbf{G_{F2}}$ (C, D), $\mathbf{G_{F3}}$ (E, F), $\mathbf{G_{F4}}$ (G, H), $\mathbf{G_{F5}}$ (I, J), $\mathbf{G_{F6}}$ (K, L), $\mathbf{G_{F7}}$ (M, N), and $\mathbf{G_{F8}}$ (O, P). To facilitate the AFM measurements the scratches shown in optical images are implemented on purpose. The black square denotes the location where the AFM characterization has been carried out.

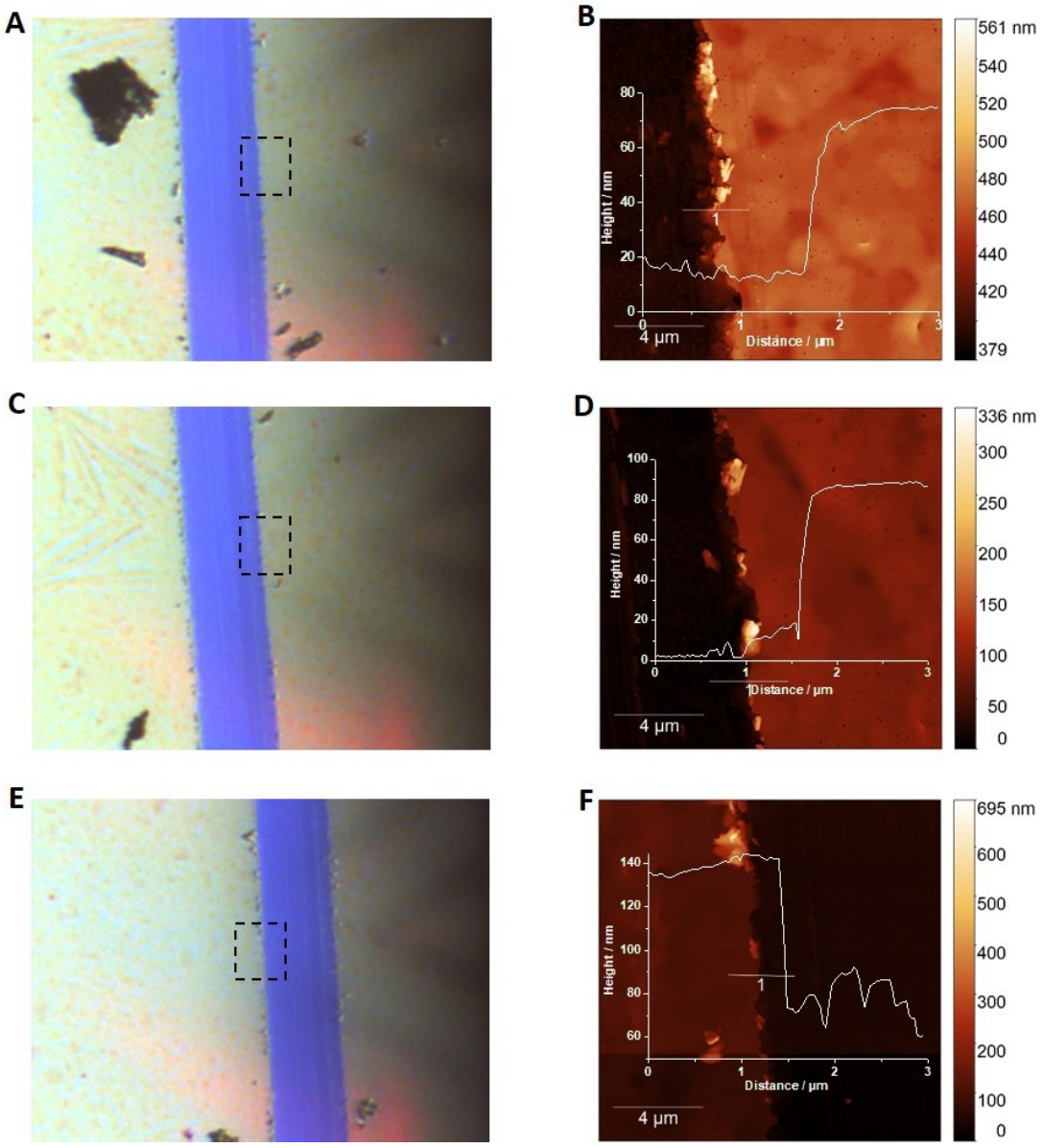
A
B
C
D
E
F
Height / nm
Distance / µm
4 µm
561 nm
336 nm
695 nm

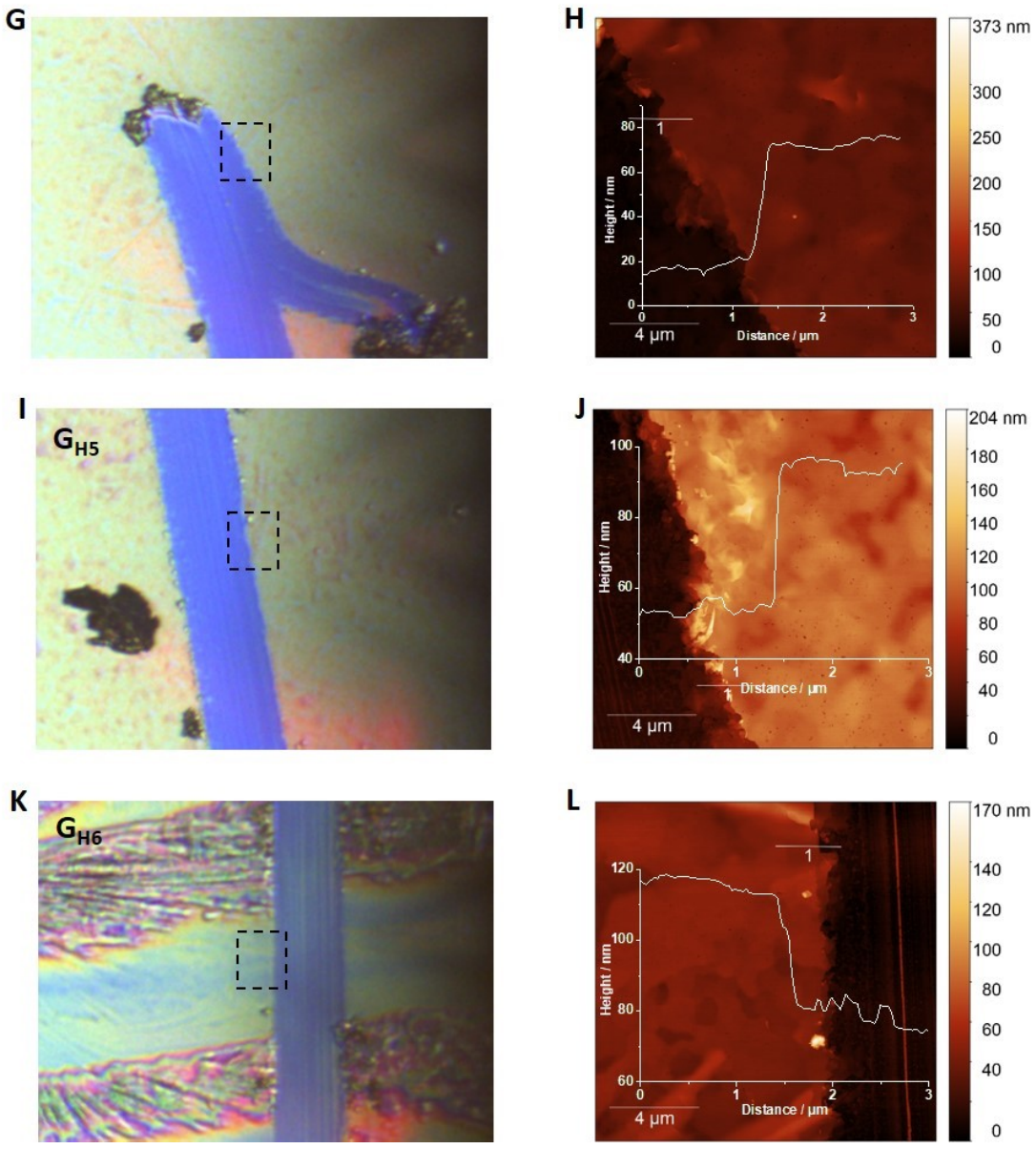

Figure S7. Optical images and corresponding AFM images of precursor film in samples $\mathbf{G_{H1}}$ (A, B), $\mathbf{G_{H2}}$ (C, D), $\mathbf{G_{H3}}$ (E, F), $\mathbf{G_{H4}}$ (G, H), $\mathbf{G_{H5}}$ (I, J), and $\mathbf{G_{H6}}$ (K, L). In order to facilitate the AFM measurements the scratches shown in optical images are implemented on purpose. The black square denotes the location where the AFM characterization has been carried out.

Removal of the silver nanoparticles. Silver nanoparticles are produced during the laser-writing process and confined to the laser-irradicated regions, presenting the identical patterns as organic addends. To visualize the regular distributions of silver nanoparticles, AFM measurements were performed on graphene samples after laser writing and subsequent removal of excess reagents, revealing a pattern-dependent arrangement of these silver nanoparticles (Figure S5 and S6). On the other hand, the resulting silver particles can be facilely removed by a two-step treatment consisting of washing with diluted nitric acid (0.3 mol/L for 10 min) and sequential ultrasonication (30W) in diluted nitric acid (1 min) and isopropanol (1min). For example, after laser writing and subsequent rinse of the residues of reagents, the letter pattern “I” remains visible as shown in the optical image (Figure S 9A) due to the generation of silver particles. This was further confirmed by AFM analysis, which showed that the pattern was composed of silver nanoparticles (Figure S6B and S6C). However, upon washing treatment by submerging the sample in diluted nitric acid (0.3 mol/L) for 10 minutes and a sequential ultrasonic treatment (30 W) in diluted nitric acid (0.3 mol/L) (1 min) and isopropanol (1 min), the patterned silver nanoparticles were eliminated (Figure S9B). The successful removal of silver nanoparticles was corroborated by AFM measurements, where the distinct letter pattern "I" was disappeared (Figure S9C).

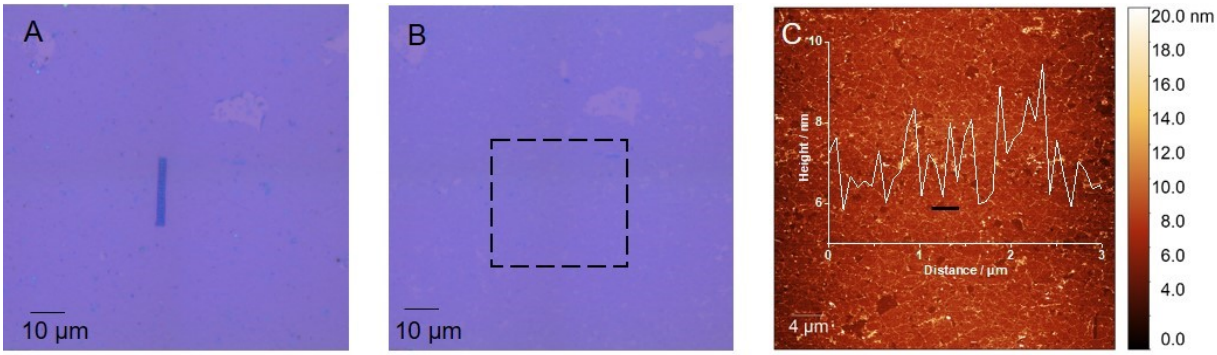

Figure S9. Optical images of $\mathbf{G_{H2}}$ before (A) and after (B) removal of silver nanoparticles and the corresponding AFM image after depletion of silver nanoparticles. The black square denotes the location where the AFM characterization has been carried out.

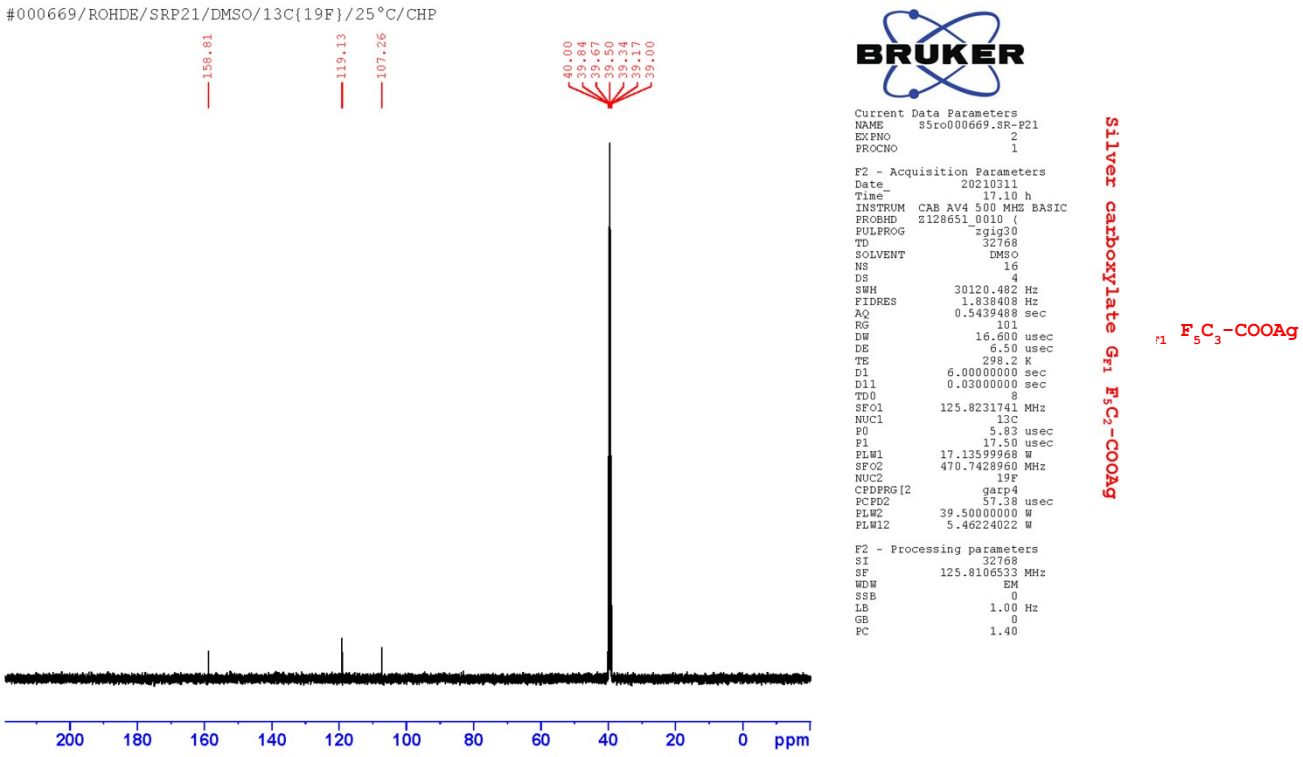

Figure S10. G_{F1}, δ_C (126 MHz, DMSO-d_6).

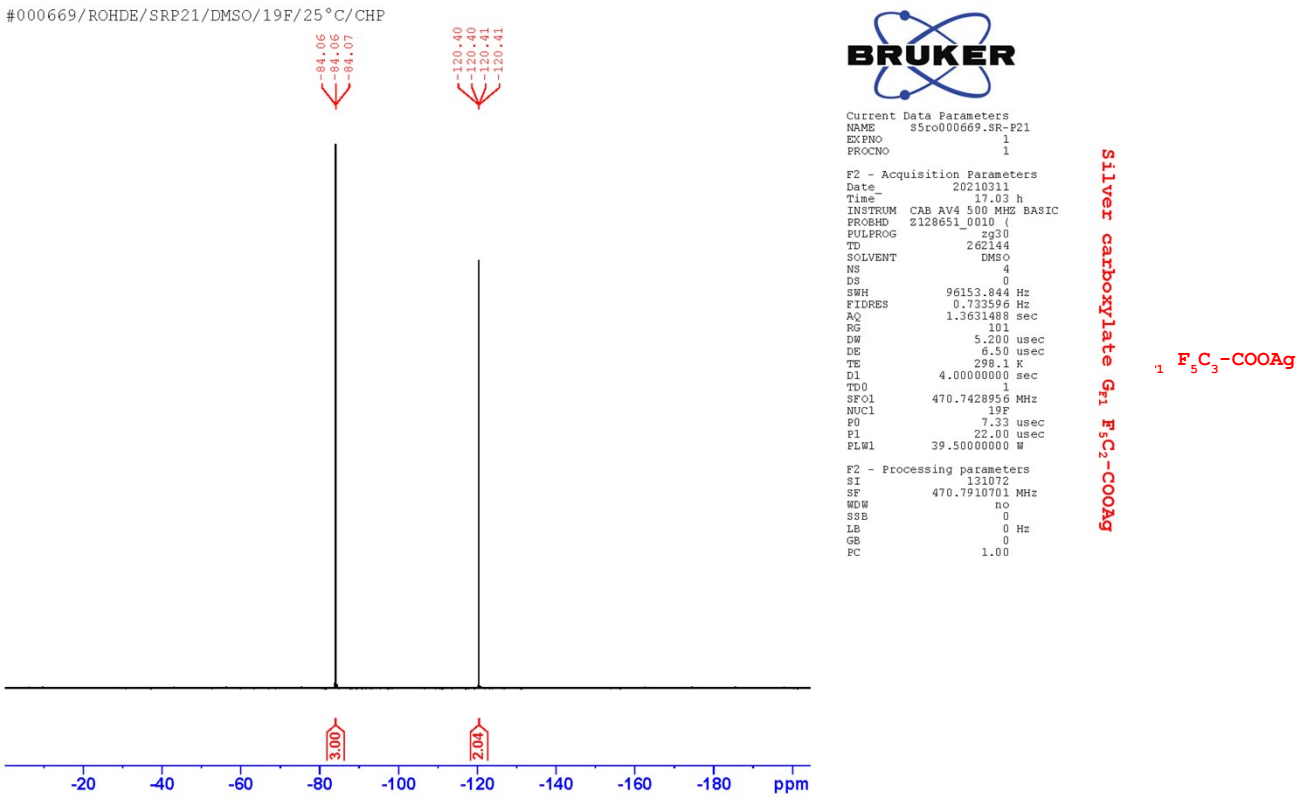

Figure S11. $G_{F1,}$ δ_F (471 MHz, DMSO-d_6).

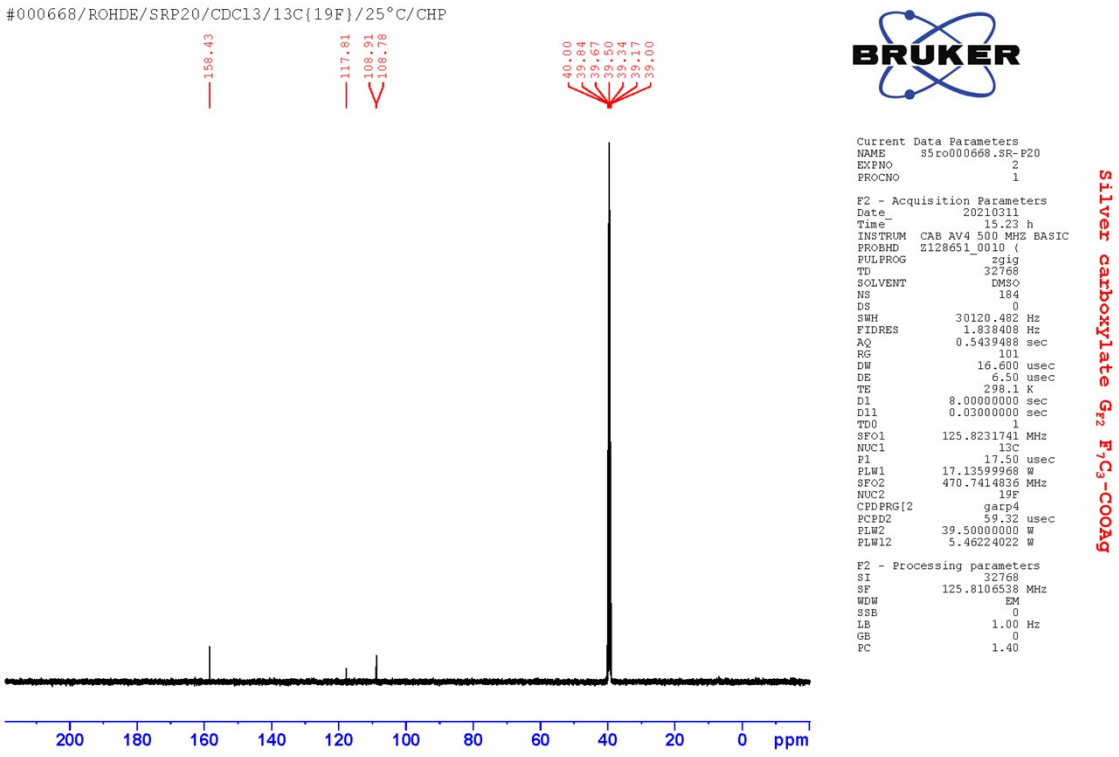

Figure S12. G_{F2}, δ_C (126 MHz, DMSO-d_6).

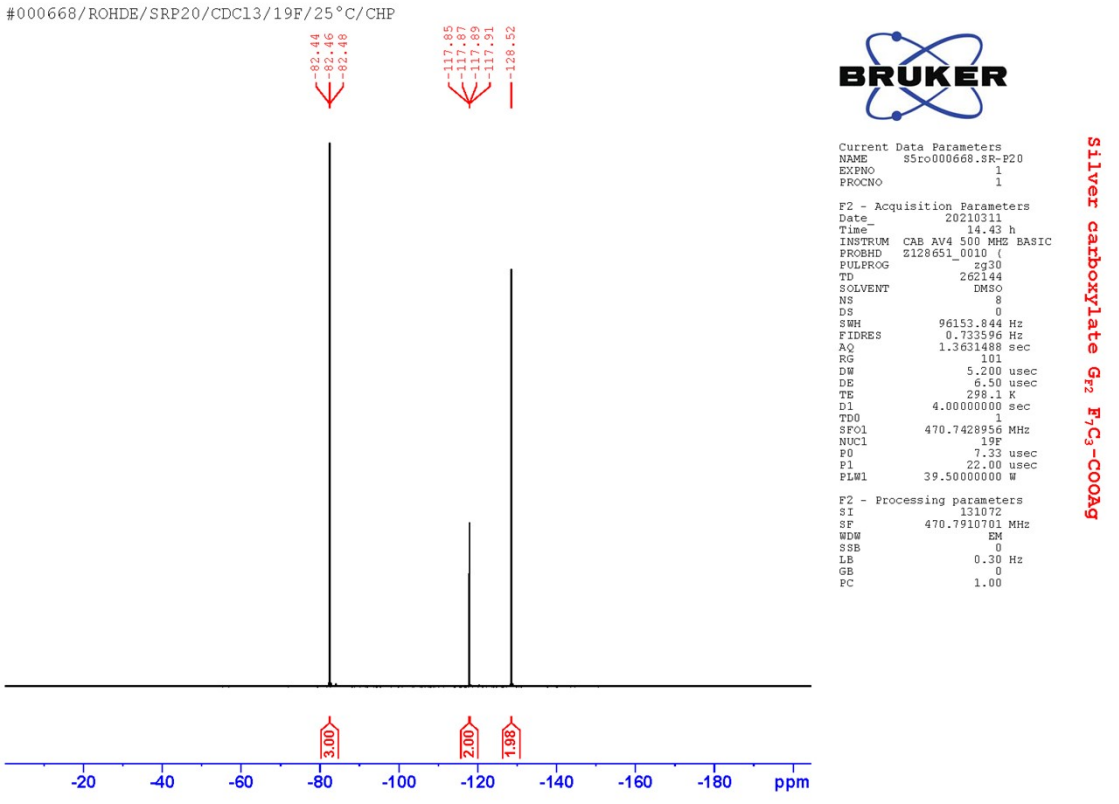

Figure S13. $G_{F2,}$ δ_F (471 MHz, DMSO-d_6).

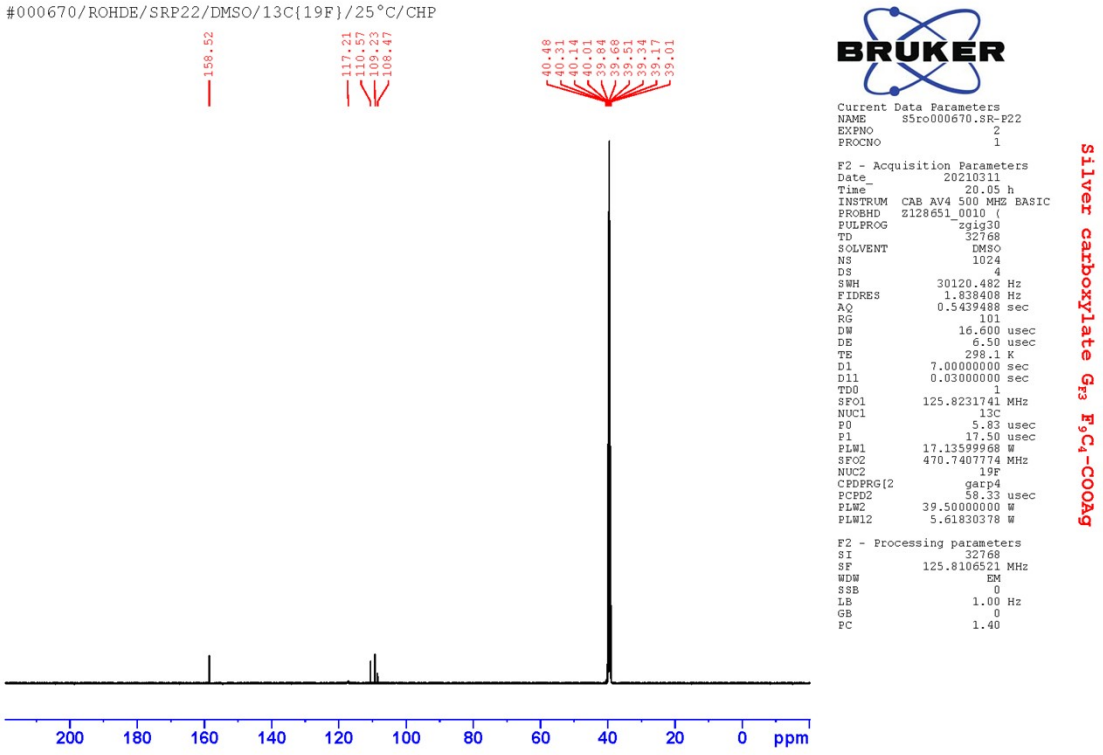

Figure S14. G_{F3}, δ_C (126 MHz, DMSO-d_6).

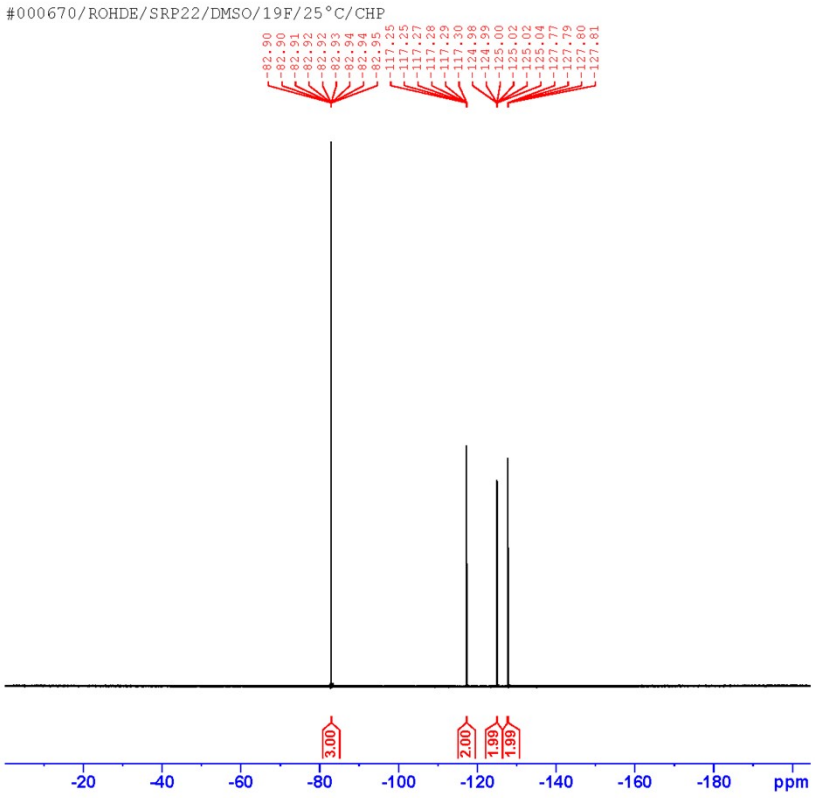

Figure S15. $G_{F3,}$ $\delta_{\mathbf{F}}$ (471 MHz, DMSO-d_6).

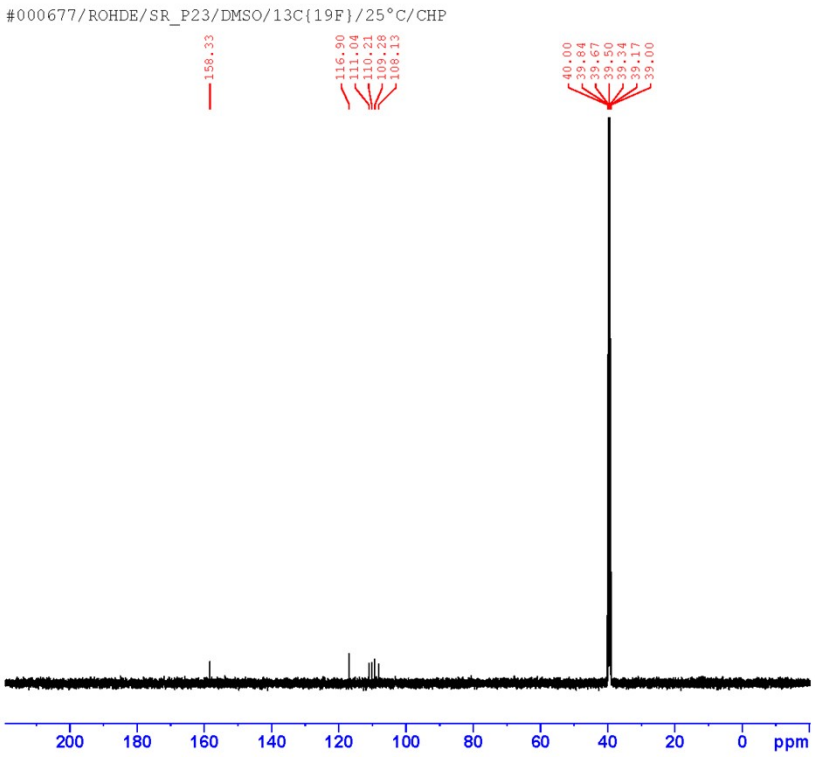

Figure S16. $G_{F4,}$ $\delta_{\mathbf{C}}$ (126 MHz, DMSO-d_6).

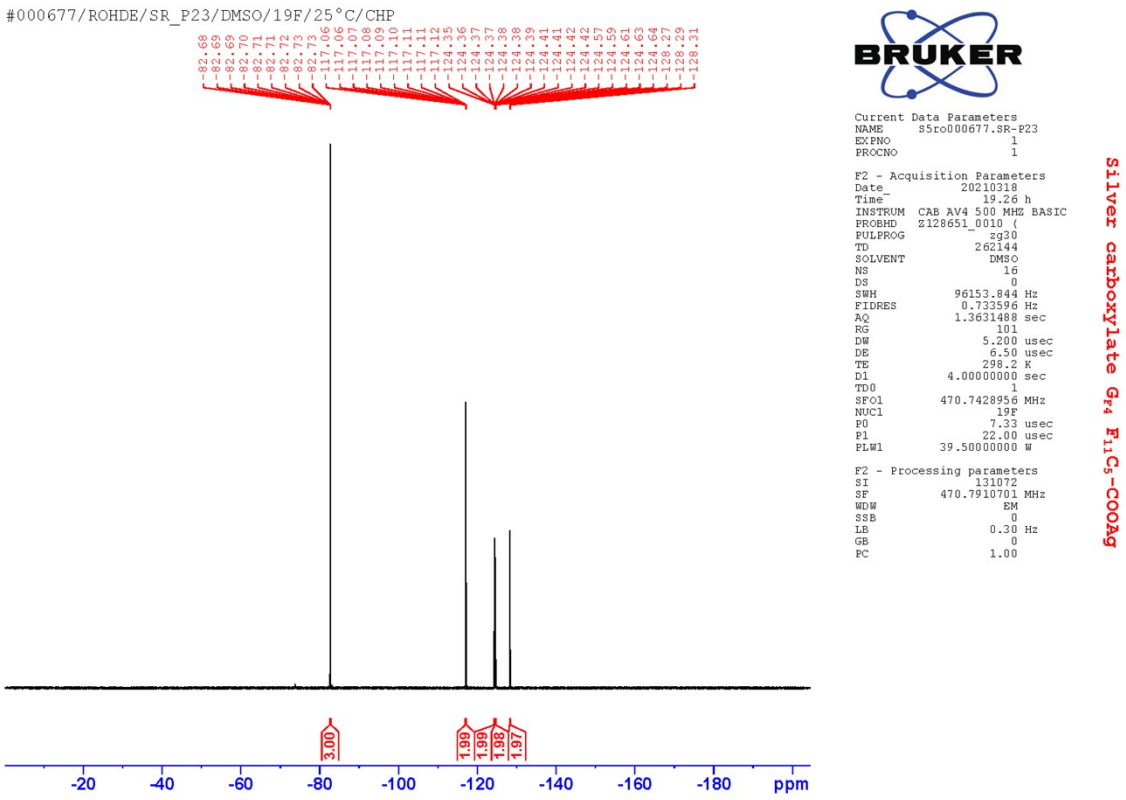

Figure S17. $G_{F4,}$ δ_F (471 MHz, DMSO-d_6).

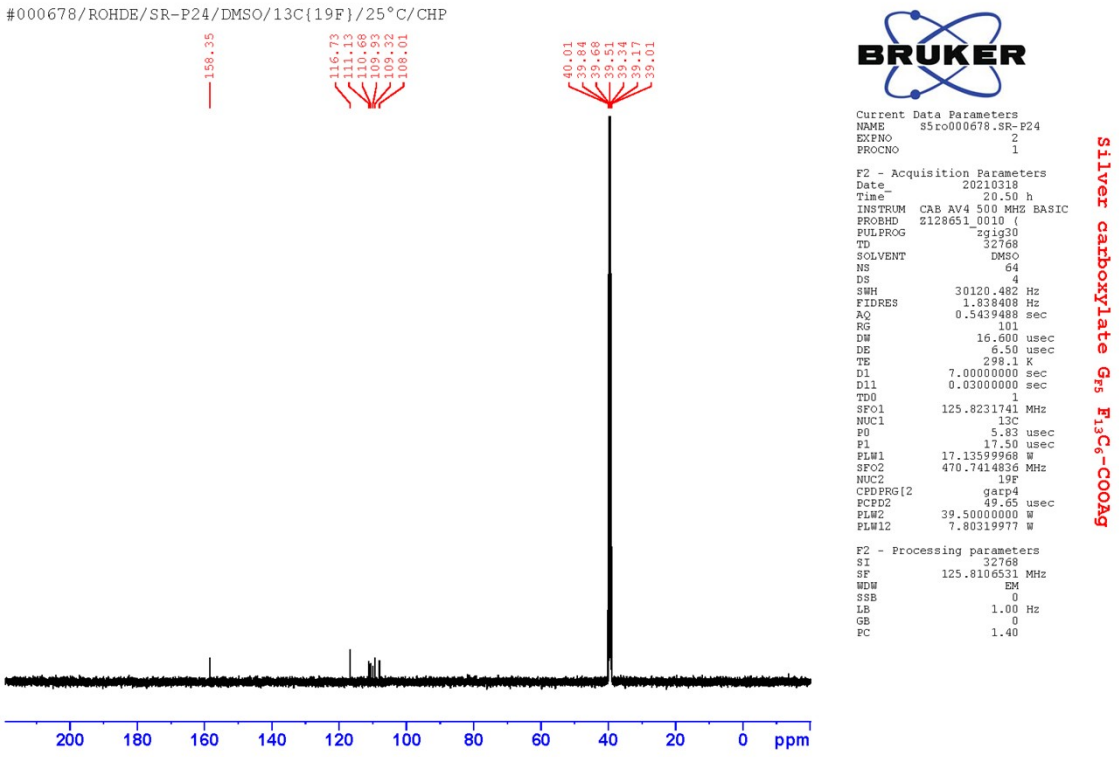

Figure S18. G_{F5}, δ_C (126 MHz, DMSO-d_6).

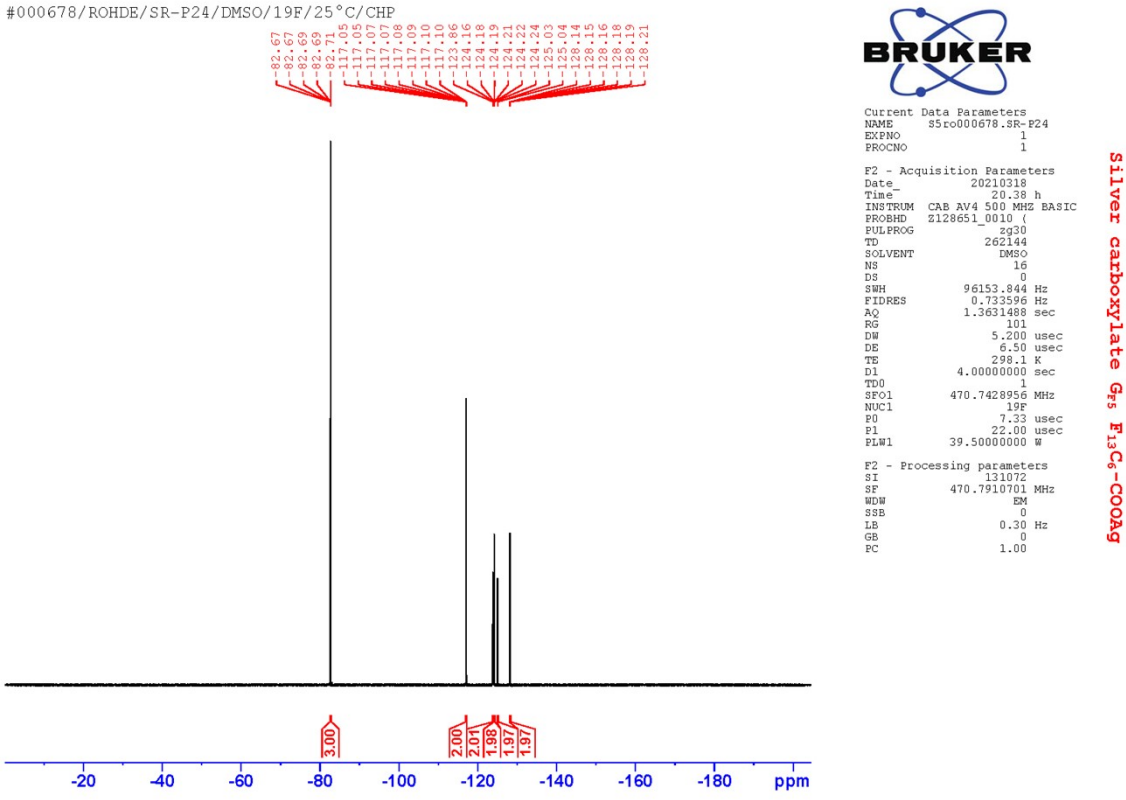

Figure S19. $G_{F5,}$ δ_F (471 MHz, DMSO-d_6).

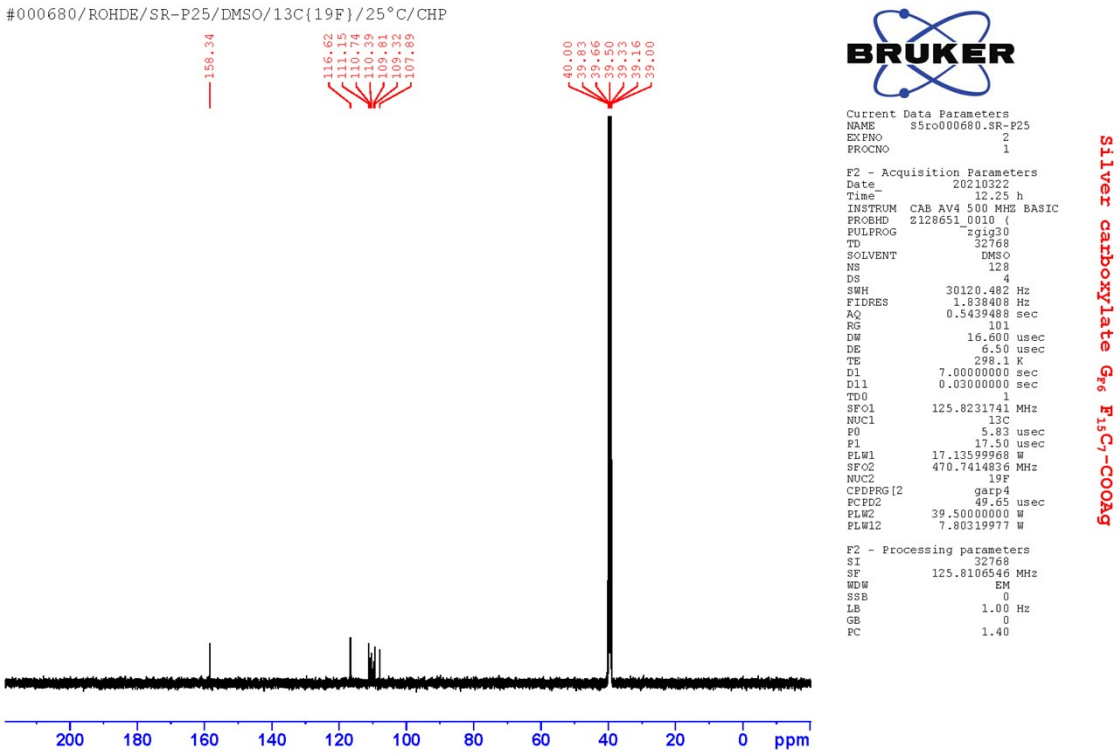

Figure S20. G_{F6}, δ_C (126 MHz, DMSO-d_6).

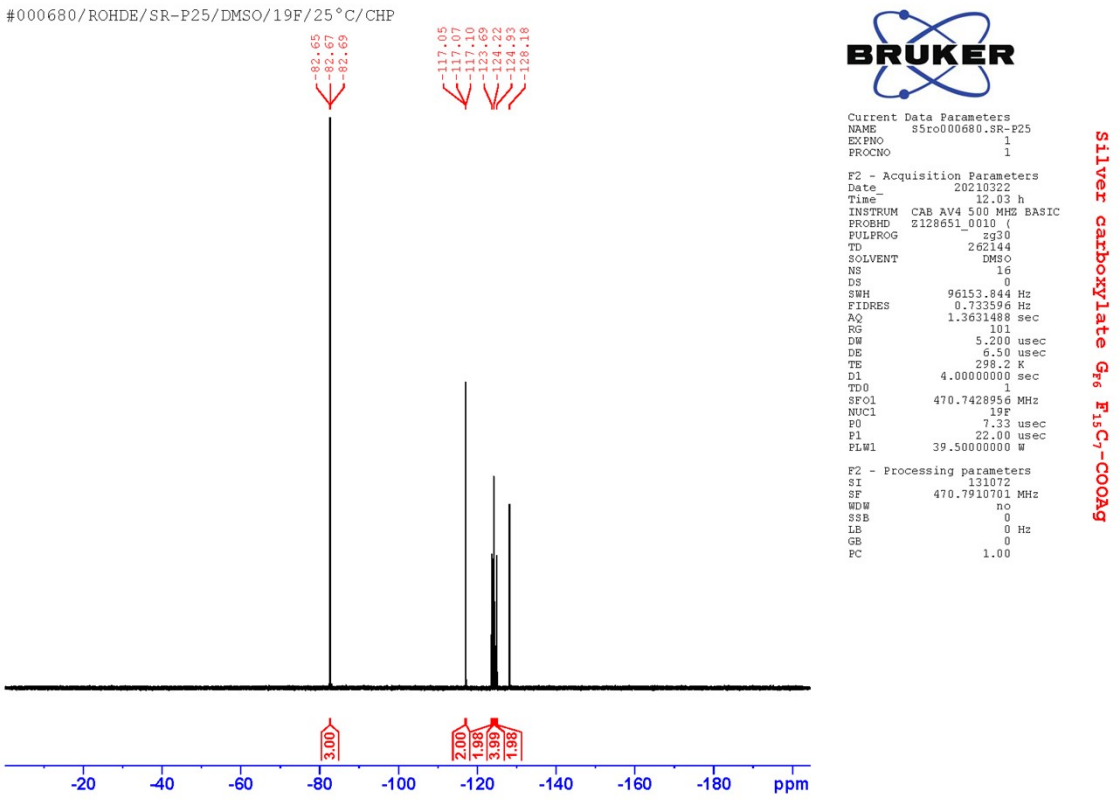

Figure S21. $G_{F6,}$ δ_F (471 MHz, DMSO-d_6).

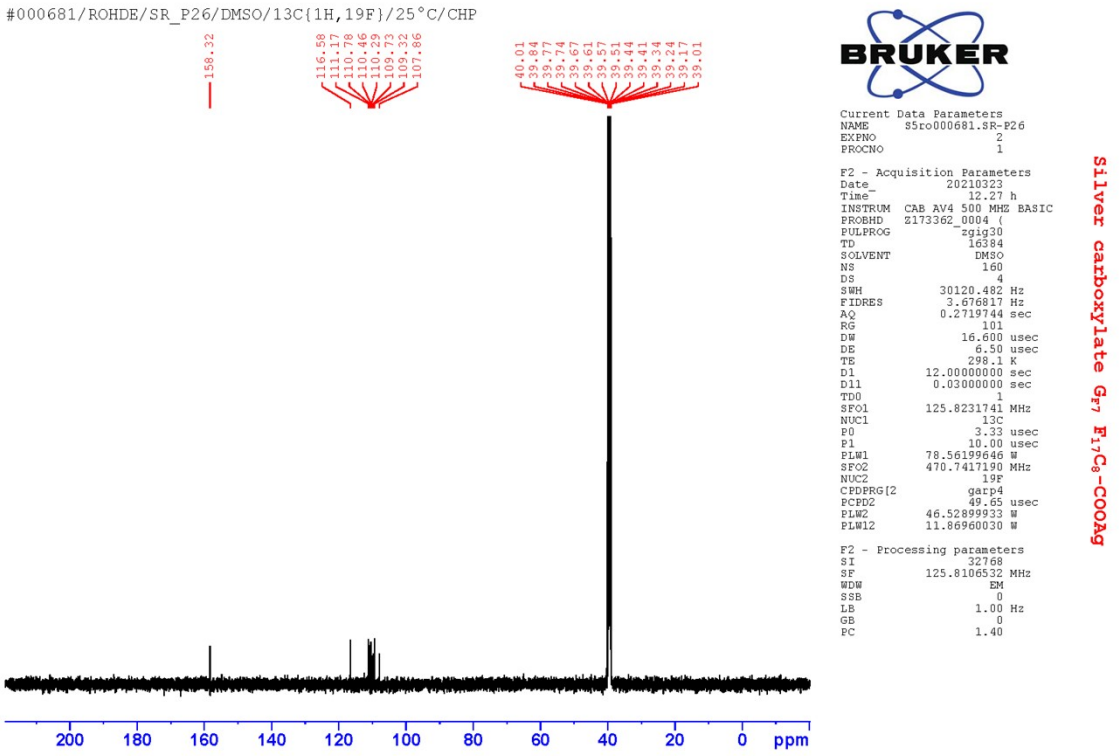

Figure S22. G_{F7}, δ_C (126 MHz, DMSO-d_6).

Figure S23. $G_{F7,}$ δ_F (471 MHz, DMSO-d_6).

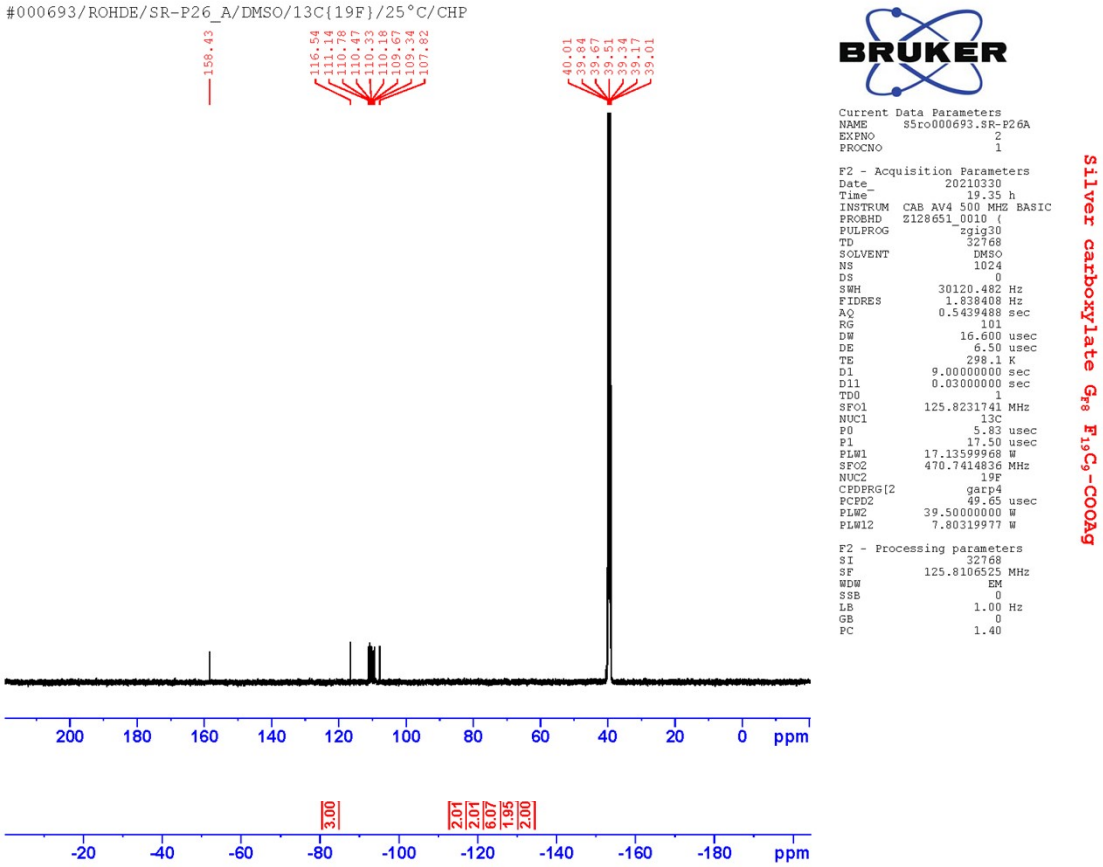

Figure S24. G_{F8}, δ_C (126 MHz, DMSO-d_6).

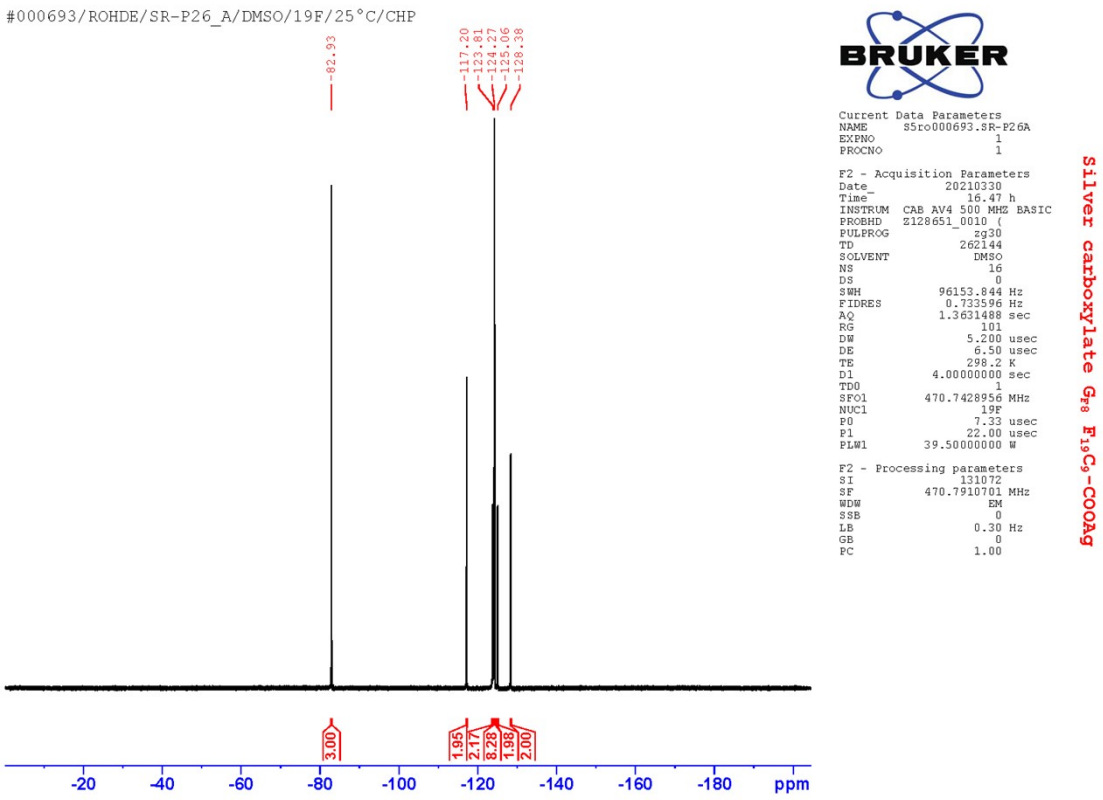

Figure S25. $G_{F8,}$ δ_F (471 MHz, DMSO-d_6).

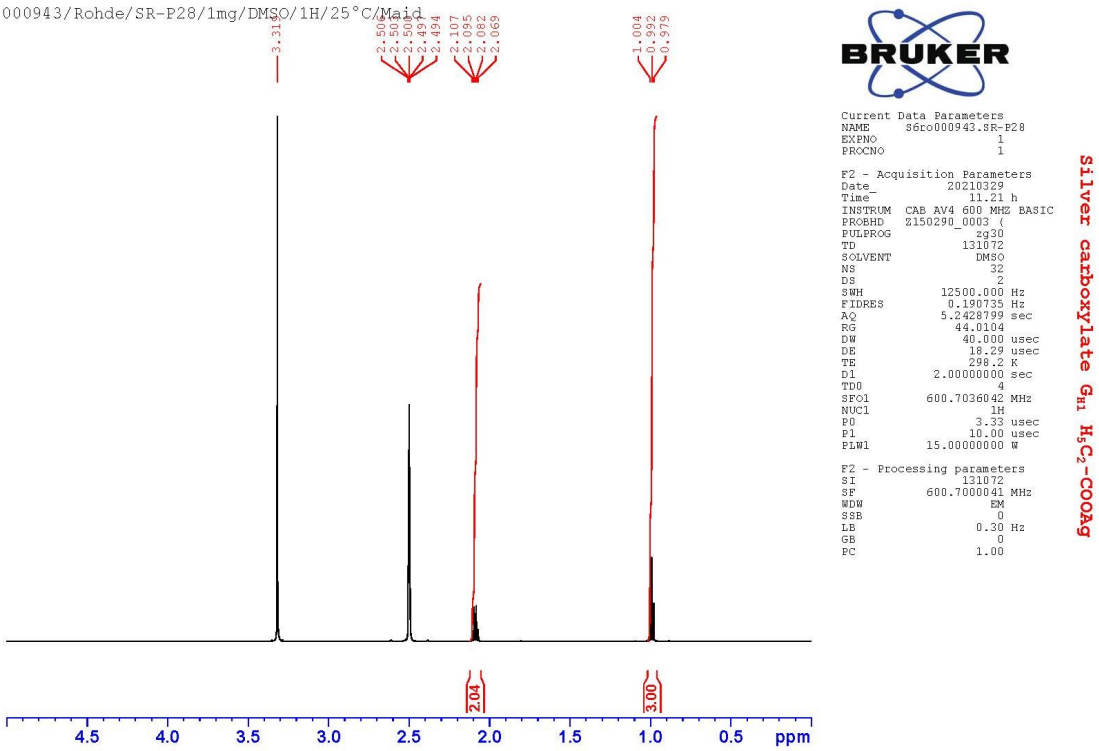

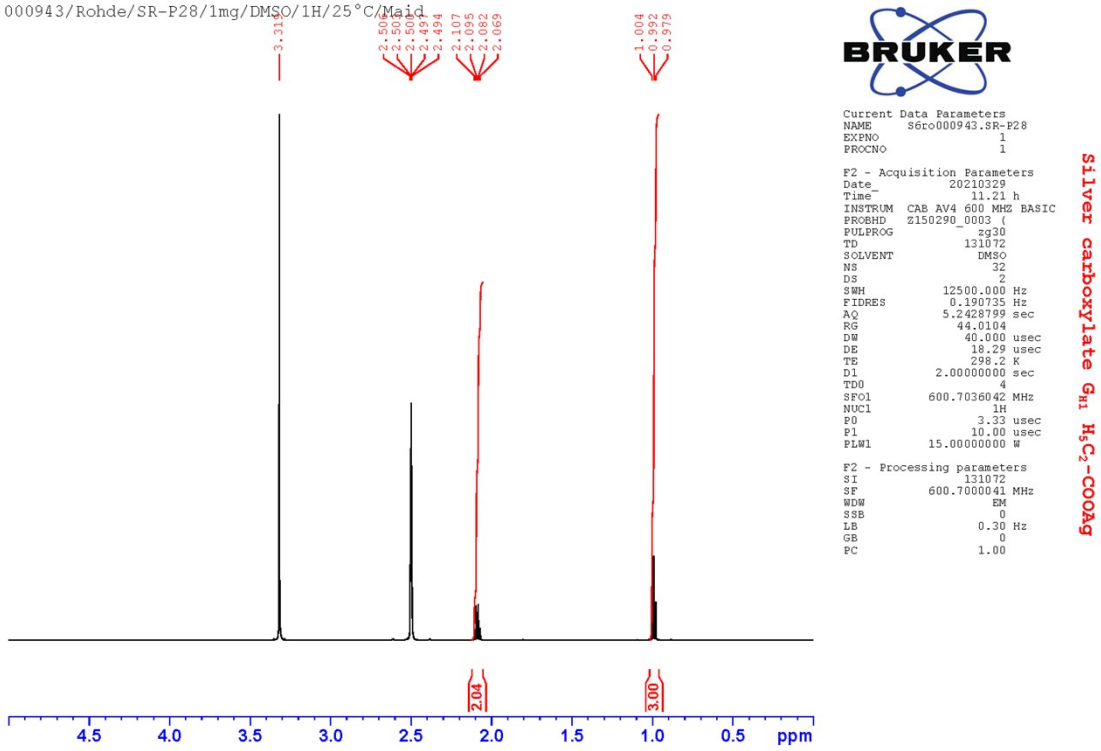

Figure S26. G_{H1}, $\delta_{\mathbf{H}}$ (600 MHz, DMSO-d_6)

Figure S27. $G_{H1,}$ $\delta_{\mathbf{C}}$ (151 MHz, DMSO-d_6).

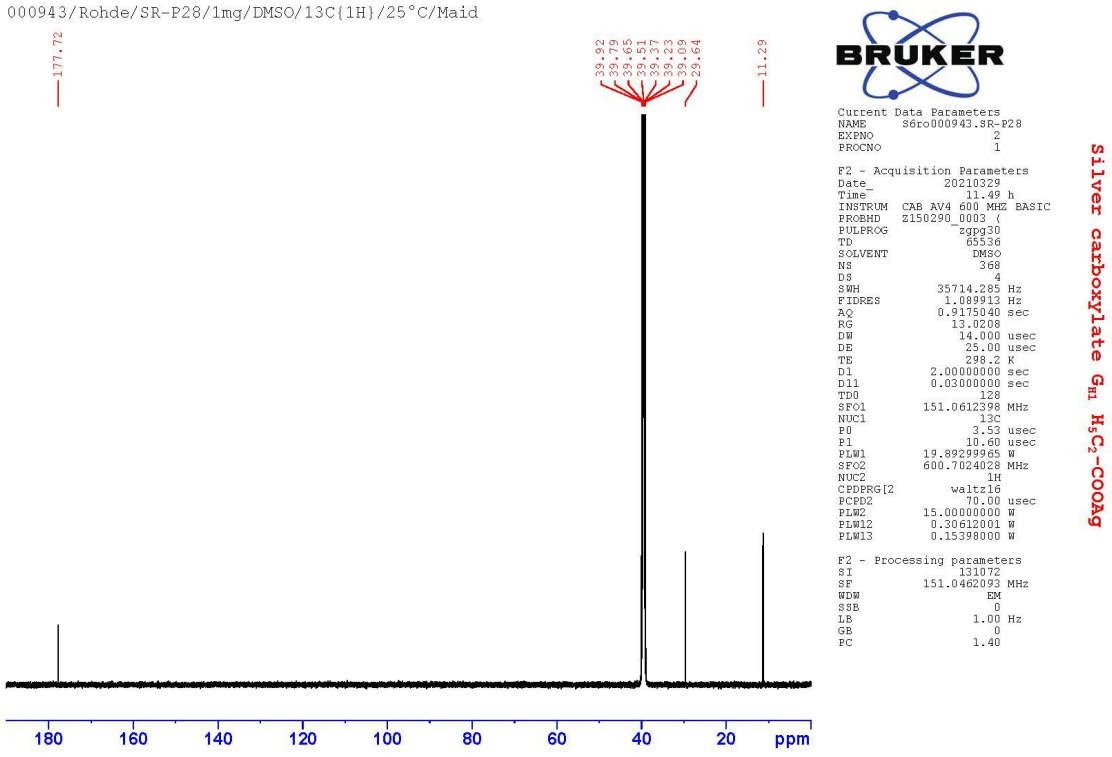

Figure S28. G_{H2}, δ_H (600 MHz, DMSO-d_6).

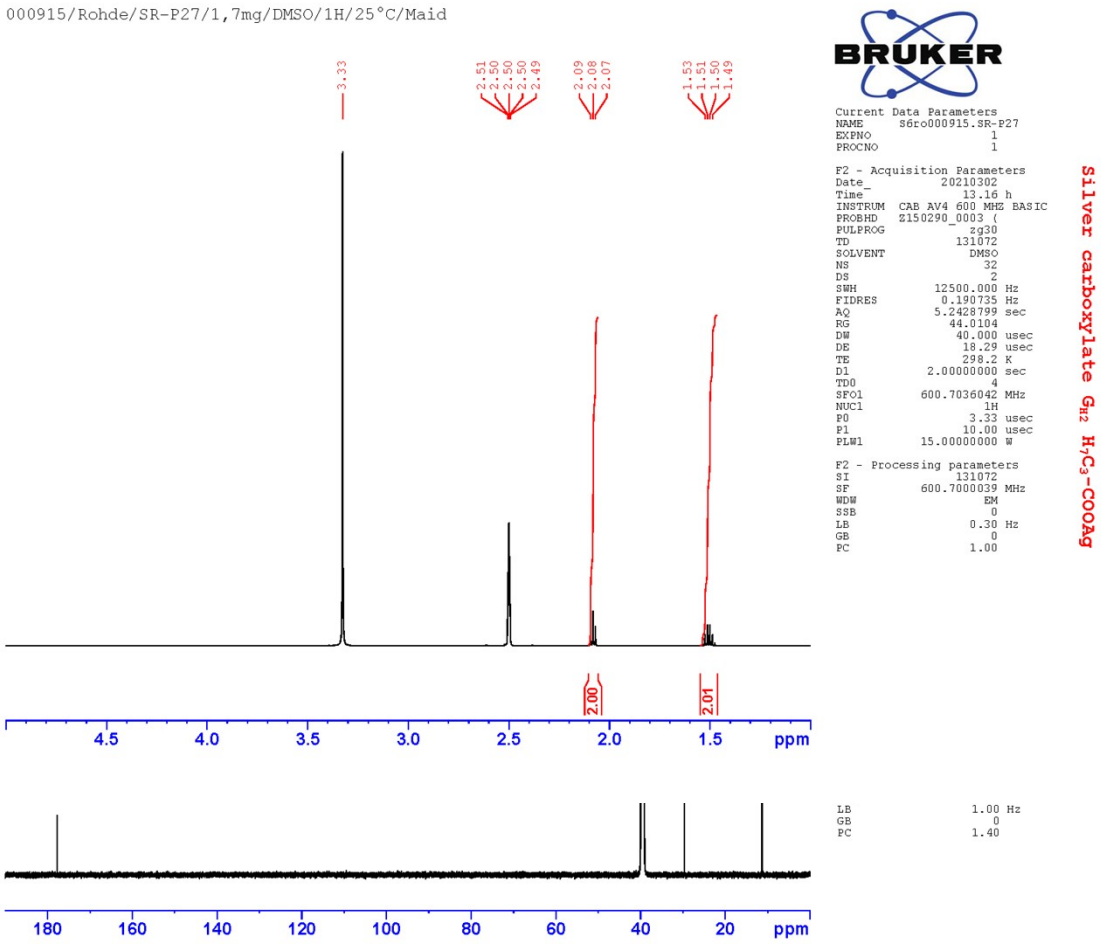

Figure S29. $G_{H2,}$ δ_C (151 MHz, DMSO-d_6).

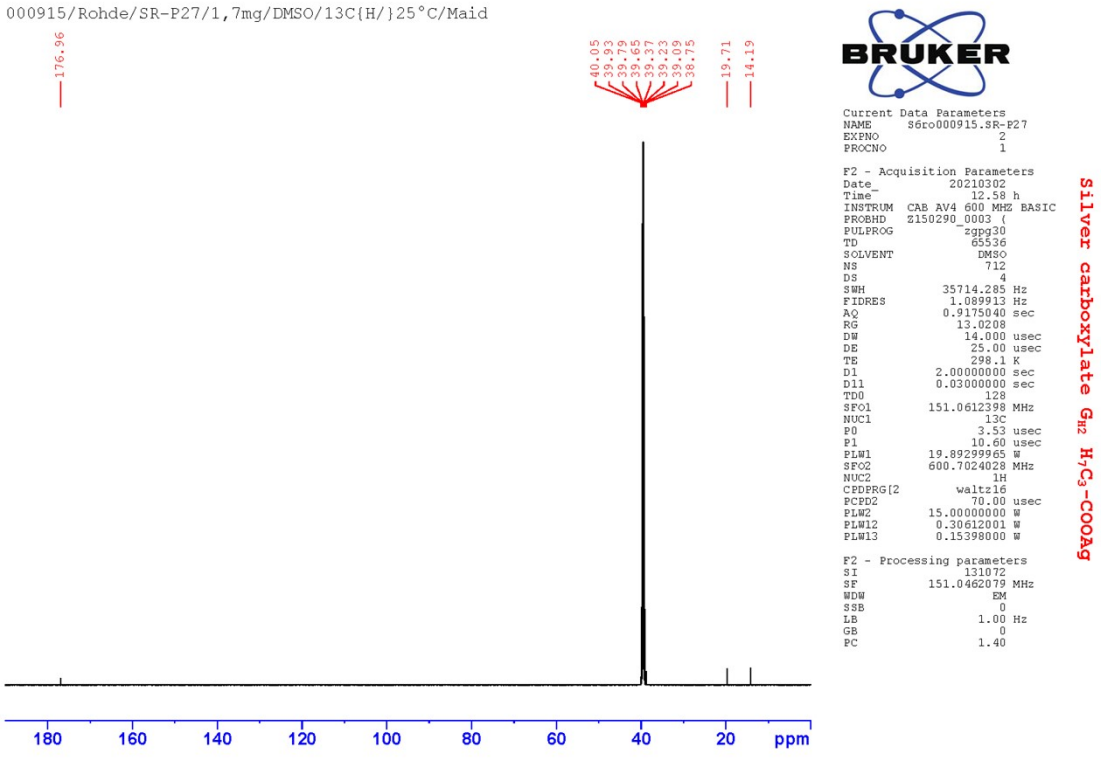

Figure S30. G_{H3}, δ_H (600 MHz, DMSO-d_6).

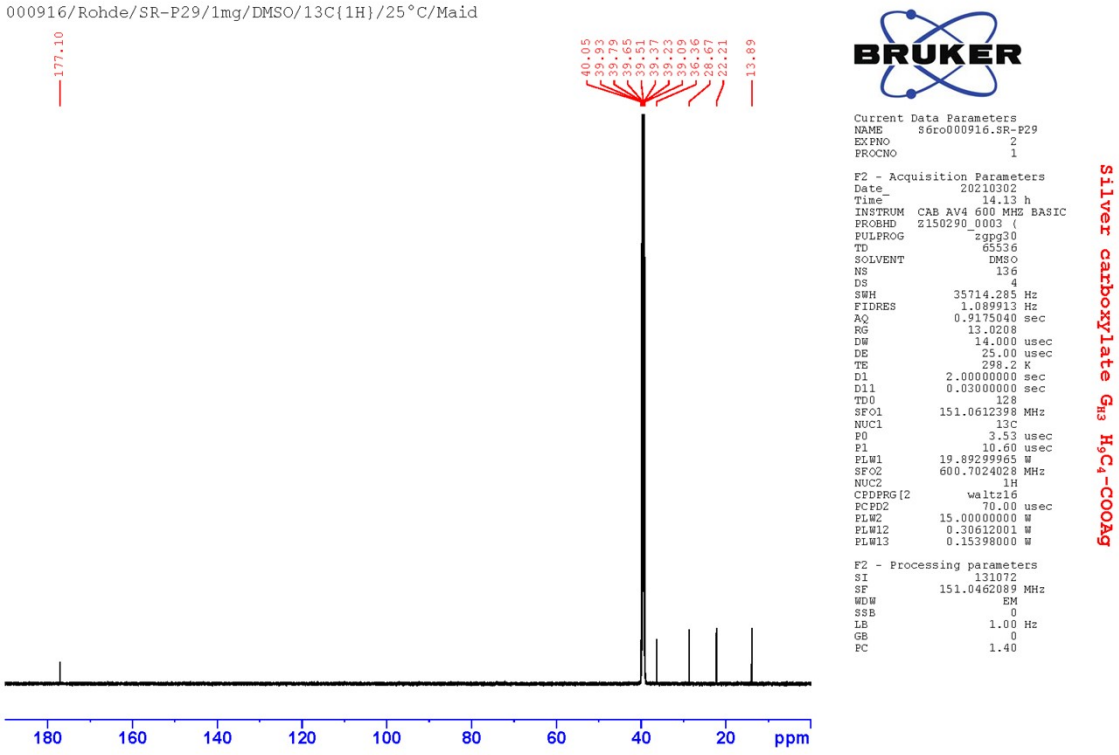

Figure S31. $G_{H3,}$ δ_C (151 MHz, DMSO-d_6).

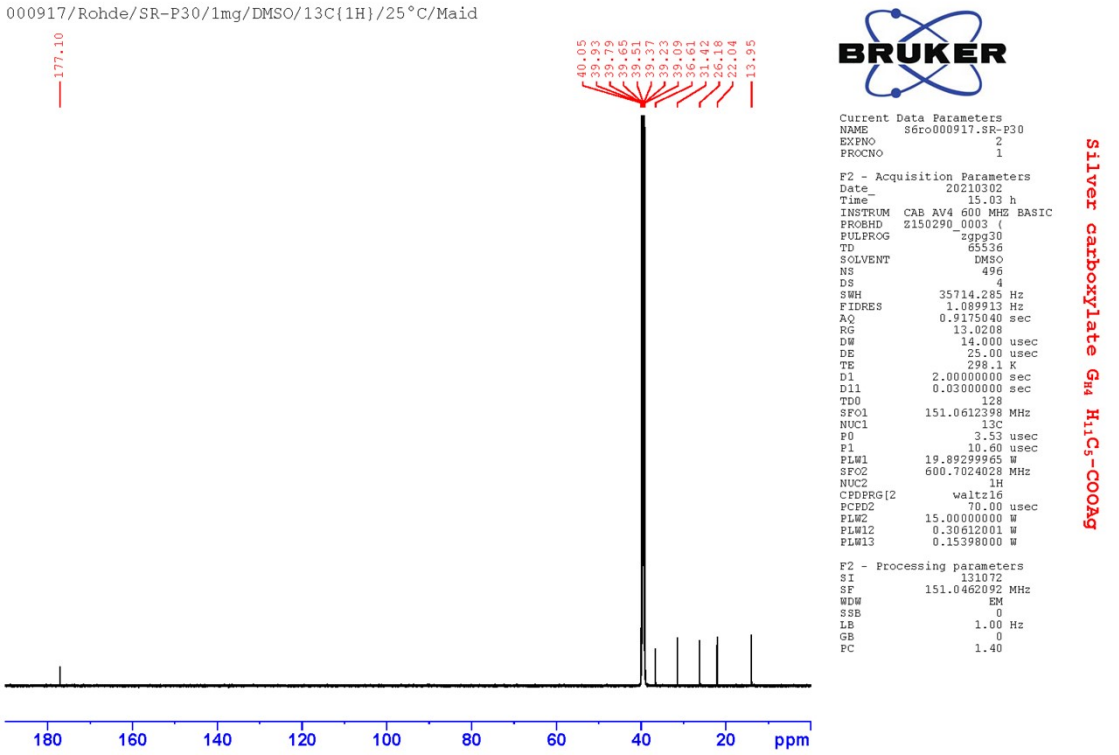

Figure S32. G_{H4}, δ_H (600 MHz, DMSO-d_6).

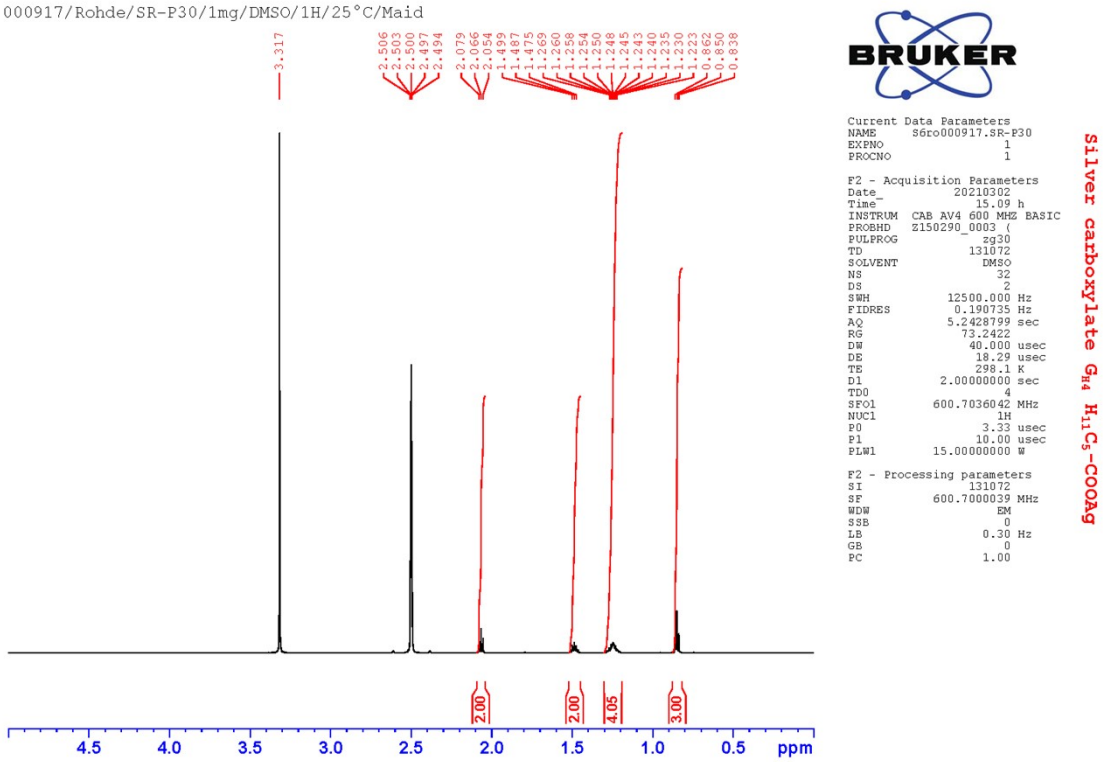

Figure S33. $G_{H4,}$ δ_C (151 MHz, DMSO-d_6)

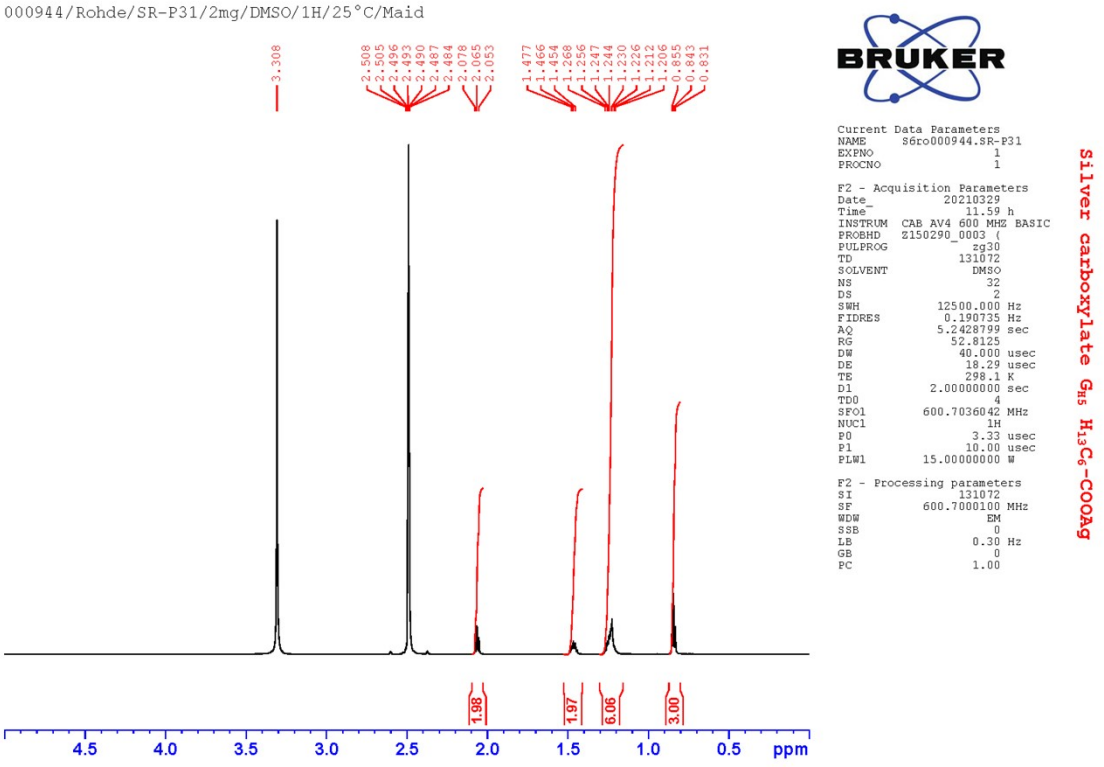

Figure S34. G_{H5}, δ_H (600 MHz, DMSO-d_6).

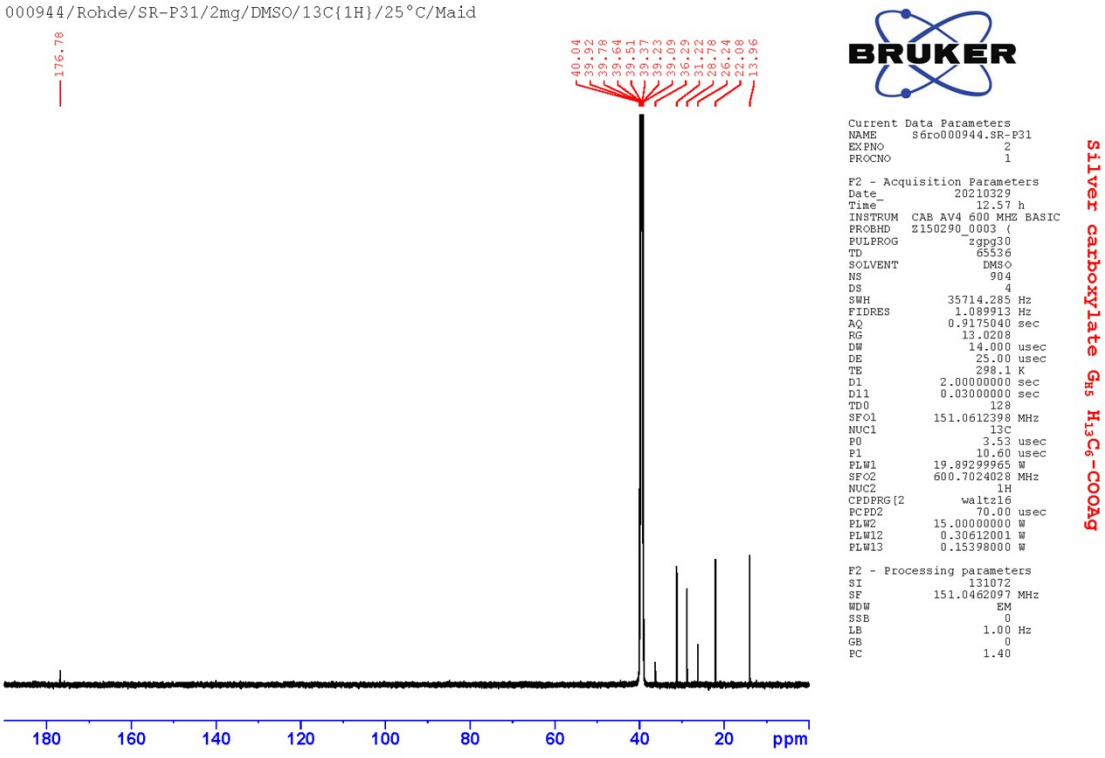

Figure S35. $G_{H5,}$ δ_C (151 MHz, DMSO-d_6).

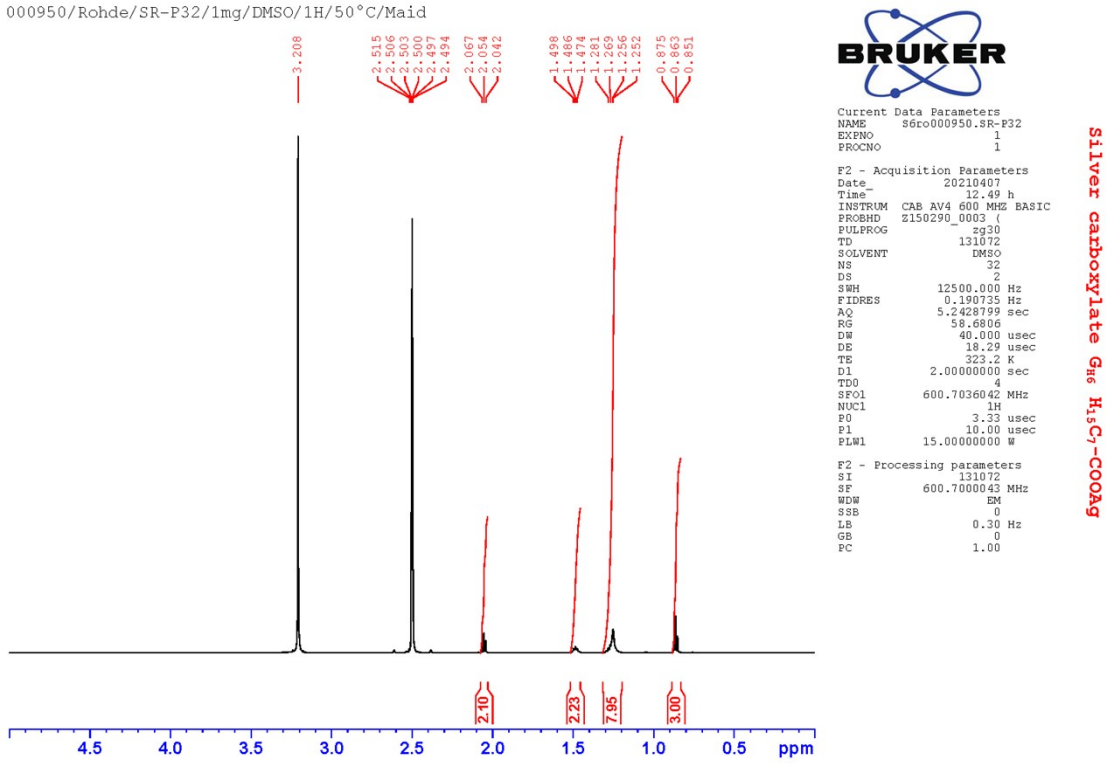

Figure S36. G_{H6}, δ_H (600 MHz, DMSO-d_6).

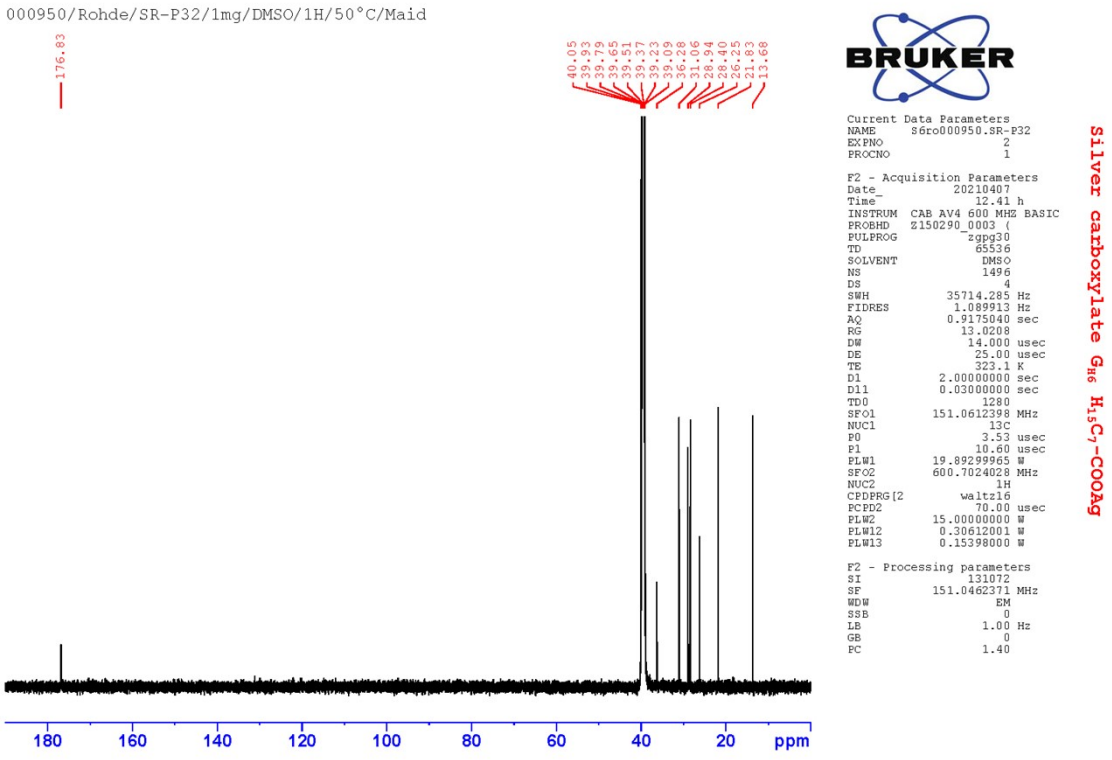

Figure S37. G_6, δ_C (151 MHz, DMSO-d_6).

Reference:

[1] E. Szlyk, R. Szczęsny, A. Wojtczak, *Dalton Trans.*, 2010, **39**, 1823-1830.

[2] E. Szłyk, I. Szymańska, A. Surdykowski, T. Głowiak, A. Wojtczak, A. Goliński, *Dalton Trans.*, 2003, 3404-3410

[3] E. Szłyk, I. Łakomska, A. Grodzicki, *Thermochim. Acta*, **1993**, 223, 207–212.

[4] J. Torroba, J. Aynsley, P. A. Tuzimoto, D. W. Bruce, *RSC Adv.*, 2012, **2**, 12866-12869

[5] E. Szłyk, Szymańska I, R. Szczęsny, *Polish J Chem.,* 2005, **79**, 627-35.